Asian Journal of Chemistry; Vol. 37, No. 1 (2025), 75-92

ASIAN JOURNAL OF CHEMISTRY

https://doi.org/10.14233/ajchem.2025.32847

DFT, Wave Function and SAR Analyses of Fexinidazole: A Drug for Sleeping Sickness

E. JIMLA PUSHPAM and J. WINFRED JEBARAJ*

Department of Chemistry, St. John's College (Affiliated to Manonmaniam Sundaranar University, Abishekapatti), Palayamkottai, Tirunelveli-627002, India

*Corresponding author: E-mail: winfred.chem@stjohnscollege.edu

Received: 7 October 2024; *Accepted*: 30 November 2024; *Published online*: 31 December 2024; AJC-21854

Fexinidazole is a newly authorized drug employed for the treatment of sleeping sickness in South Africa. The characteristics of drug molecule in the gaseous form were calculated using Gaussian 16W software, employing the DFT/B3LYP/6-311++G(d,p) level of theory. The absence of imaginary frequency indicates the full convergence and optimization. Mulliken charge analysis was carried out. The ESP elucidates the suitability of the nitro group for electrophilic assault and FMO demonstrates that it is an electron donor. The NLO investigation reveals that it is a good NLO candidate and the NBO studies reveals that it is highly stable. The NCI interaction demonstrates that it exhibits van der Waals and steric repulsion forces. IFCT, STM and aromaticity determinations were performed. The S0 → S3 and S4 are having charge transfer (CT) type of excitation as per the HEI investigation. The SAR activity was examined using 5UFG protein, leading to the identification of two promising molecules.

Keywords: Fexinidazole, Density functional theory, Electrostatic potential, Non-covalent interaction, Structure activity relationship.

INTRODUCTION

The disease known as sleeping sickness or human African trypanosomiasis, is more common in rural parts of sub-Saharan Africa. It is brought on by a parasite called *Trypanosoma brucei gambiense*. Glossina tsetse flies are the ones who disperse it. The sickness common in Western and Central Africa is caused by the microbe *T. b. gambiense* [1-3]. The disease has been known for more than 100 years and reported that about 55 million people in 36 countries were at risk [4] in 1999 and that about 50,000 new cases were reported each year [5]. Before 1920s, only a few drugs, like pentamidine and suramin, were used as first-choice medicines to treat early-stage sickness. In later years, melarsoprol, a drug based on arsenic that was developed in 1949, was still the primary drug used to treat late-phase sleeping sickness. Then, DFMO was used to treat late-phase sleeping sickness [6].

Now days, fexinidazole is the most common drug used to treat sleeping sickness. It works well against both early and late stages of illnesses. It has also been shown to help fight Chagas disease, which affects millions of people around the world [7]. It belongs to the categories of nitroimidazole and antiparasitic compounds [8]. This was made into a drug by the FDA in the USA in July 2021 [9]. Being an important molecule, DFT work are not yet known. So, we tried to explore the structural properties and reactivity of this molecule. Within the chemical, biological and material sciences lies the field of theoretical chemistry [10]. In organic chemistry, it is helpful to realise the structure of the molecule, reaction mechanisms and various physical properties [11,12].

COMPUTATIONAL METHODS

The 2D structure of fexinidazole is drafted using the Chemsketch software package [13]. The ground state with minimum energy of the molecule was optimized with the help of Avogadro tool [14]. The optimization process is a crucial step in decreasing the computational time and providing the exact outcomes. The Gaussian 16W package was used to validate all the experiments in the gaseous phase [15]. The Gaussview 06 facilitates the visualization of files which are sent and received [16]. The density functional theory (DFT) was used for all the calculations [17], therefore, all computations used Becke's three parameter functional (B3LYP) approach with the 6-311++G(d,p) basis set [18]. Using DFT formulae along with B3LYP is the best way to get accurate results [19]. The fact that the imaginary

This is an open access journal, and articles are distributed under the terms of the Attribution 4.0 International (CC BY 4.0) License. This license lets others distribute, remix, tweak, and build upon your work, even commercially, as long as they credit the author for the original creation. You must give appropriate credit, provide a link to the license, and indicate if changes were made.

frequency is not present proves that the molecule has been optimized and validated by the GaussSum 3.0 tool [20]. The wave function analysis was performed using the Multiwfn 3.8 software program [21]. The thermodynamic properties were analyzed with the help of the Shermo program [22]. The VMD 1.9.3 tool was adopted to illustrate some graphical results [23].

RESULTS AND DISCUSSION

Electronic structure determination: Fexinidazole drug ($C_{12}H_{13}N_3O_3S$) is composed of 32 atoms and 146 electrons. It is a neutral and singlet system. Table-1 shows the list of atoms and whereas Table-2 lists the bond distance (Å), bond angle (°) and dihedral angles (°) of fexinidazole. Fig. 1 shows the 2D and 3D and images of the molecule in full convergence and optimization. For docking analysis, Discovery Studio Visualizer software (https://www.3ds.com/products/biovia/reference-center) was used for the preparation of protein and to view the docking results. PyRx was used to dock the ligand molecules and the prepared proteins [24].

The connection between carbon atom 15 (15C) and hydrogen atom 29 (29H) has the shortest length, measuring 1.078 Å. The most considerable bond distance (1.836 Å) is between the atoms 7S and 8C. The molecule of interest exhibits a bond angle of 100.8º, the shortest among all the bond angles. This particular bond angle is formed by carbon atom 6, sulphur atom 7 and carbon atom 8 (6C-7S-8C). The bond angle of 128.7º is particularly notable in the 14C-12N-16C position. A dihedral angle measures the angle formed by the intersection of two planes. The existence of synperiplanar (SP), synclinal (SC), antiperiplanar (AP) and anticlinal (AC) planar structures in this molecule is indicated by the dihedral angle values. The values were consistent with the values reported earlier [26-28].

TABLE-1
LIST OF ATOMS OF FEXINIDAZOLE

1	2	3	4	5	6	7	8	9	10	11	12	13	14	15	16
C	**C**	**C**	**C**	**C**	**C**	**S**	**C**	**O**	**C**	**C**	**N**	**N**	**C**	**C**	**C**
17	18	19	20	21	22	23	24	25	26	27	28	29	30	31	32
N	**O**	**O**	**H**	**H**	**H**	**H**	**H**	**H**	**H**	**H**	**H**	**H**	**H**	**H**	**H**

TABLE-2
ELECTRONIC STRUCTURE DETAILS OF FEXINIDAZOLE

S. No	Atom set	Bond distance (Å)	Atom set	Bond angle (°)	Atom set	Dihedral angle (°)	Planarity
1	1C-2C	1.396	2C-1C-3C	120.0	3C-1C-2C-4C	0.0	+SP
2	1C-3C	1.399	2C-1C-9O	124.5	3C-1C-2C-20H	180.0	+AP
3	1C-9O	1.371	3C-1C-9O	115.5	9O-1C-2C-4C	179.7	+AP
4	2C-4C	1.397	1C-2C-4C	119.5	9O-1C-2C-20H	-0.4	-SP
5	2C-20H	1.082	1C-2C-20H	121.5	2C-1C-3C-5C	0.1	+SP
6	3C-5C	1.387	4C-2C-20H	119.1	2C-1C-3C-21H	179.8	+AP
7	3C-21H	1.083	1C-3C-5C	120.0	9O-1C-3C-5C	-179.6	-AP
8	4C-6C	1.394	1C-3C-21H	118.9	9O-1C-3C-21H	0.1	+SP
9	4C-22H	1.084	5C-3C-21H	121.2	2C-1C-9O-10C	-0.8	-SP
10	5C-6C	1.402	2C-4C-6C	121.1	3C-1C-9O-10C	178.9	+AP
11	5C-23H	1.084	2C-4C-22H	119.4	1C-2C-4C-6C	0.2	+SP
12	6C-7S	1.796	6C-4C-22H	119.5	1C-2C-4C-22H	-179.6	-AP
13	7S-8C	1.836	3C-5C-6C	120.8	20H-2C-4C-6C	-179.8	-AP
14	8C-24H	1.091	3C-5C-23H	119.7	20H-2C-4C-22H	0.5	+SP
15	8C-25H	1.090	6C-5C-23H	119.5	1C-3C-5C-6C	-0.4	-SP
16	8C-26H	1.090	4C-6C-5C	118.7	1C-3C-5C-23H	179.2	+AP
17	9O-10C	1.429	4C-6C-7S	120.6	21H-3C-5C-6C	179.8	+AP
18	10C-11C	1.493	5C-6C-7S	120.7	21H-3C-5C-23H	-0.6	-SP
19	10C-27H	1.093	6C-7S-8C	100.8	2C-4C-6C-5C	-0.5	-SP
20	10C-28H	1.098	7S-8C24H	106.3	2C-4C-6C-7S	-178.4	-AP
21	11C-12N	1.363	7S-8C-25H	110.9	22H-4C-6C-5C	179.3	+AP
22	11C-13N	1.329	7S-8C-26H	110.9	22H-4C-6C-7S	1.3	+SP
23	12N-14C	1.386	24H-8C-25H	109.3	3C-5C-6C-4C	0.6	+SP
24	12N-16C	1.468	24H-8C-26H	109.2	3C-5C-6C-7S	178.6	+AP
25	13N-15C	1.354	25H-8C-26H	110.2	23H-5C-6C-4C	-179.0	-AP
26	14C-15C	1.379	1C-9O-10C	118.4	23H-5C-6C-7S	-1.0	-SP
27	14C-17N	1.427	9O-10C-11C	108.8	4C-6C-7S-8C	-94.7	-AC
28	15C-29H	1.078	9O-10C-27H	111.2	5C-6C-7S-8C	87.3	+SC
29	16C-30H	1.086	9O-10C-28H	109.9	6C-7S-8C-24H	-179.7	-AP
30	16C-31H	1.088	11C-10C-27H	106.9	6C-7S-8C-25H	61.7	+SC
31	16C-32H	1.088	11C-10C-28H	111.3	6C-7S-8C-26H	-61.1	-SC
32	17N-18O	1.233	27H-10C-28H	108.8	1C-9O-10C-11C	178.3	+AP
33	17N-19O	1.227	10C-11C-12N	124.6	1C-9O-10C-27H	60.9	+SC

34	10C-11C-13N	122.8	1C-9O-10C-28H	-59.6	-SC
35	12N-11C-13N	112.5	9O-10C-11C-12N	63.2	+SC
36	11C-12N-14C	104.9	9O-10C-11C-13N	-118.1	-AC
37	11C-12N-16C	126.4	27H-10C-11C-12N	-176.6	-AP
38	14C-12N-16C	128.7	27H-10C-11C-13N	2.1	+SP
39	11C-13N-15C	106.0	28H-10C-11C-12N	-58.0	-SC
40	12N-14C-15C	107.2	28H-10C-11C-13N	120.7	+AC
41	12N-14C-17N	124.9	10C-11C-12N-14C	179.1	+AP
42	15C-14C-17N	128.0	10C-11C-12N-16C	-0.9	-SP
43	13N-15C-14C	109.4	13N-11C-12N-14C	0.2	+SP
44	13N-15C-29H	123.3	13N-11C-12N-16C	-179.7	-AP
45	14C-15C-29H	127.3	10C-11C-13N-15C	-179.0	-AP
46	12N-16C-30H	108.0	12N-11C-13N-15C	-0.1	-SP
47	12N-16C-31H	110.1	11C-12N-14C-15C	-0.3	-SP
48	12N-16C-32H	110.1	11C-12N-14C-17N	179.4	+AP
49	30H-16C-31H	109.3	16C-12N-14C-15C	179.7	+AP
50	30H-16C-32H	110.6	16C-12N-14C-17N	-0.6	-SP
51	31H-16C-32H	108.8	11C-12N-16C-30H	-0.3	-SP
52	14C-17N-18O	118.3	11C-12N-16C-31H	-119.5	-AC
53	14C-17N-19O	116.8	11C-12N-16C-32H	120.5	+AC
54	18O-17N-19O	124.9	14C-12N-16C-30H	179.7	+AP
55			14C-12N-16C-31H	60.5	+SC
56			14C-12N-16C-32H	-59.4	-SC
57			11C-13N-15C-14C	-0.1	-SP
58			11C-13N-15C-29H	-179.9	-AP
59			12N-14C-15C-13N	0.2	+SP
60			12N-14C-15C-29H	180.0	+AP
61			17N-14C-15C-13N	-179.4	-AP
62			17N-14C-15C-29H	0.3	+SP
63			12N-14C-17N-18O	0.0	+SP
64			12N-14C-17N-19O	179.9	+AP
65			15C-14C-17N-18O	179.6	+AP
66			15C-14C-17N-19O	-0.5	-SP

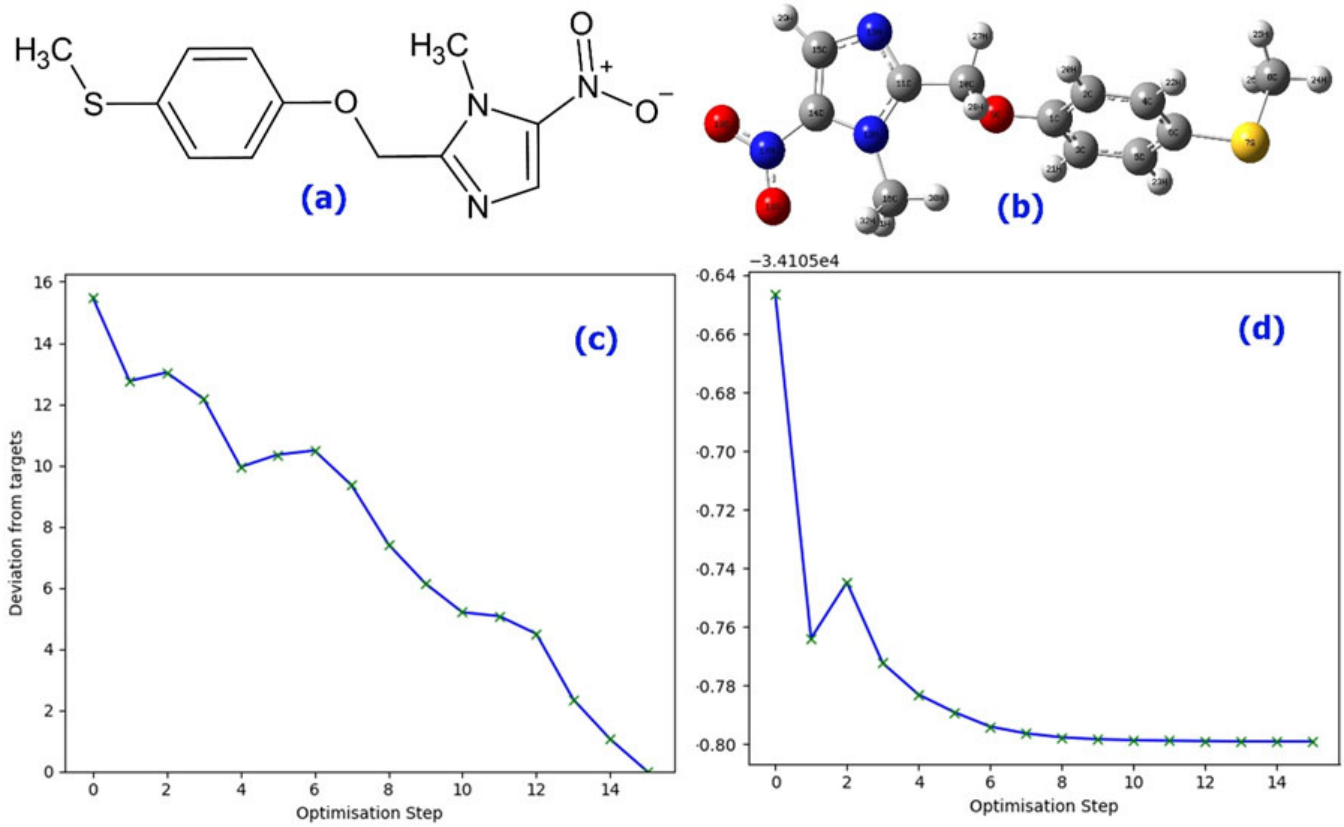

Fig. 1. (a) 2D (b) optimized 3D (c) full optimisation (d) complete convergence images of fexinidazole

Analysis of Mulliken charge: Accurate atomic charge estimation is essential for applying quantum chemical calculations. It impacts the dipole moment, molecular structure, polarizability, acidity behaviour and other physical qualities. Table-3 presents the Mulliken charges obtained for the molecule being studied using the same level of theory. A visual depiction (Fig. 2) is also produced to enhance comprehension using the data from Table-3.

Based on Table-3 and Fig. 2, it was observed that 6C has a high positive charge (1.2615 a.u.) since it is coordinated with a sulphur atom, which is an electron-withdrawing element, while 4C has a minor charge (-0.8501 a.u.). A positive charge is placed on 19O (0.0043 a.u.) and the other two oxygen atoms (9O and 18O) have negative charges. The sulphur atom (7S) has a negative charge of -0.1470 a.u. All nitrogen atoms have negative charges; the order is 17N < 13N < 12N. Each hydrogen atom possesses a positive charge. A low charge of 0.1498 a.u. is assigned to 30H, whereas a high charge of 0.2487 a.u. is assigned to 29H.

Electrostatic potential map: The MEP (Fig. 3a) is depicted as a three-dimensional map. This tool displays the probable locations where the electrophilic attack is expected on a molecule when point reagents are present. The contour map is a straightforward tool that forecasts the potential interactions between various geometries. In general, the colour red indicates the areas with the most damaging charge (electrophilic attack zones) [29]. Blue symbolizes the area of highest positivity, specifically the regions where nucleophilic attacks occur [30]. The order of colours is as follows: red, orange, yellow, green, light blue and blue colour [31,32]. The MEP, molecular electrostatic potential is precisely defined as [33]:

$$V(r) = \sum \frac{Z_A}{|R_A - r|} - \int \frac{\rho(r')}{|r' - r|} dr \quad (1)$$

where Z_A represents the electric charge of nucleus A, situated at position R_A; r′ is a dummy variable used for integration. These maps have a colour scheme of -4.566 e^{-2} a.u. (deepest red) to 4.566 e^{-2} a.u. (deepest blue) in the compound. The colour

TABLE-3
MULLIKEN CHARGE VALUES OF FEXINIDAZOLE

S. No.	Atoms	Charge (a.u.)	S. No.	Atoms	Charge (a.u.)	S. No.	Atoms	Charge (a.u.)	S. No.	Atoms	Charge (a.u.)
1	1C	-0.4301	9	9O	-0.0343	17	17N	-0.3646	25	25H	0.1802
2	2C	0.2993	10	10C	-0.4034	18	18O	-0.0031	26	26H	0.1791
3	3C	-0.1971	11	11C	-0.4202	19	19O	0.0043	27	27H	0.2161
4	4C	-0.8501	12	12N	-0.0113	20	20H	0.1739	28	28H	0.2009
5	5C	-0.3071	13	13N	-0.0355	21	21H	0.1910	29	29H	0.2487
6	6C	1.2615	14	14C	-0.3447	22	22H	0.2130	30	30H	0.1498
7	7S	-0.1470	15	15C	0.6162	23	23H	0.1955	31	31H	0.2164
8	8C	-0.7484	16	16C	-0.4221	24	24H	0.1674	32	32H	0.2054

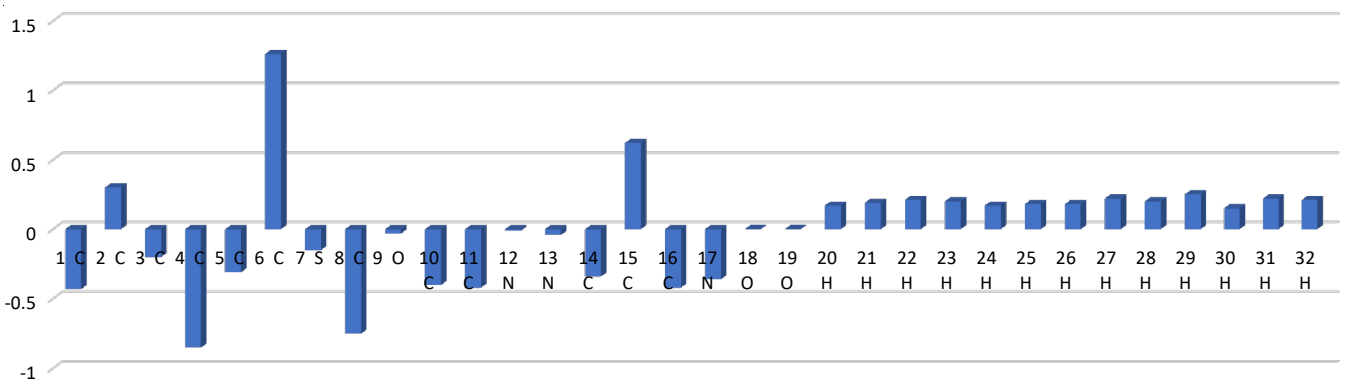

Fig. 2. Mulliken charge distribution of fexinidazole

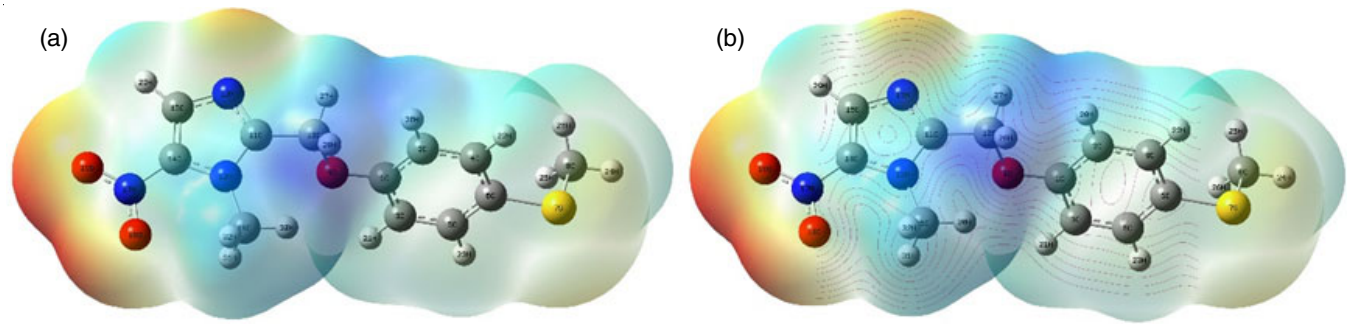

Fig. 3. (a) ESP (b) Contour diagram of fexinidazole

blue represents the most crucial attraction, whereas the red colour represents the most significant aversion. This finding indicates that the nitro group's oxygen atoms are coated in a solid red colour, which makes it the favoured site for electrophilic attack. As can be seen from the contour Fig. 3b graphic, every atom is included in the contour map.

Frontier energy gap: The HOMO-LUMO gap refers to the energy differential that exists between the HOMO and LUMO orbitals. Determining softness, hardness, ionization potential, electron affinity, electronegativity, *etc.* is crucial. The values for the target molecule are computed using the identical theoretical methodology and their visual representations are presented in Fig. 4.

Theoretically, the energy gap was calculated as 3.5102 eV to function as an electron donor. The HOMO and LUMO values were used to determine physical parameters such as ionization potential, electron affinity, electronegativity, chemical potential, chemical hardness, chemical softness, electrophilicity index, electron accepting capability, electron-donating capability and optical softness. Table-4 shows that the molecule is complex since the chemical hardness (1.7551 eV) is greater than the chemical softness (0.5698 eV). The electron-donating capacity (8.9038 eV) is higher than the electron-accepting capacity (4.1908 eV), demonstrating that in the gaseous form, the molecule is an electron donor. The optical softness value is quantified as 0.2849 eV. The molecule has a narrow energy gap in its gaseous state, leading to the heightened chemical reactivity and facilitating charge transfer. This property contributes to the biological activity of the molecule [34].

Impact of temperature on entropy (S), heat capacity at constant volume (CV) and heat capacity at constant pressure (CP): The Shermo program determines the influence of temperature on entropy (S), heat capacity at constant volume (CV) and heat capacity at constant pressure (CP). The above characteristics were evaluated using vibrational analysis and statistical thermodynamics [35]. From 100 to 1000 K, Table-5 and Fig. 5 show that there is a positive relationship between temperature and the magnitude of these thermodynamic functions. The following equations (polynomial fitting equations) are generated for this computation:

TABLE-4
THE HOMO, LUMO AND OTHER PARAMETERS OF FEXINIDAZOLE

Parameter	Formula [Ref. 25]	Charge (eV)
HOMO		-6.4681
LUMO		-2.9579
Energy gap (ΔE)		3.5102
Ionisation potential (I)	$I = - E_{HOMO}$	6.4681
Electron affinity (A)	$A = - E_{LUMO}$	2.9579
Electronegativity (χ)	$\chi = \frac{I+A}{2}$	4.713
Chemical potential (μ)	$\mu = - (\chi)$	-4.713
Chemical hardness (η)	$\eta = \frac{I-A}{2}$	1.7551
Chemical softness (S)	$S = \frac{1}{\eta}$	0.5698
Electrophilicity index (ω)	$\omega = \frac{\mu^2}{2\eta}$	6.3279
Electron accepting capability (ω^+)	$\omega^+ = \frac{(I+3A)^2}{16(I-A)}$	4.1908
Electron donating capability (ω^-)	$\omega^- = \frac{(3I+A)^2}{16(I-A)}$	8.9038
Net electrophilicity ($\Delta\omega^{\pm}$)	$\Delta\omega^{\pm} = (\omega^+ - \omega^-)$	-4.713
Global softness (s)	$s = \frac{1}{2\eta}$	0.2849
$\Delta E_{Back\ donation}$	$\Delta E = \frac{-\eta}{4}$	-0.4388
Nucleophilicity index (N)	$N = \frac{1}{\omega}$	0.158
Additional electronic charge (ΔN_{max})	$\Delta N_{max} = \frac{-\mu}{\eta}$	2.6853
Optical softness (σ_0)	$\sigma_o = \frac{1}{\Delta E}$	0.2849

$$S\ (y) = 68.9274 + 0.2412\ T - 5.2754\ e^{-5}\ T^2\ (R^2 = 0.9999)$$

$$CV\ (y) = 7.0111 + 0.2306\ T - 9.4980\ e^{-5}\ T^2\ (R^2 = 9993)$$

$$CP\ (y) = 8.9982 + 0.2306\ T - 9.4979\ e^{-5}\ T^2\ (R^2 = 0.9993)$$

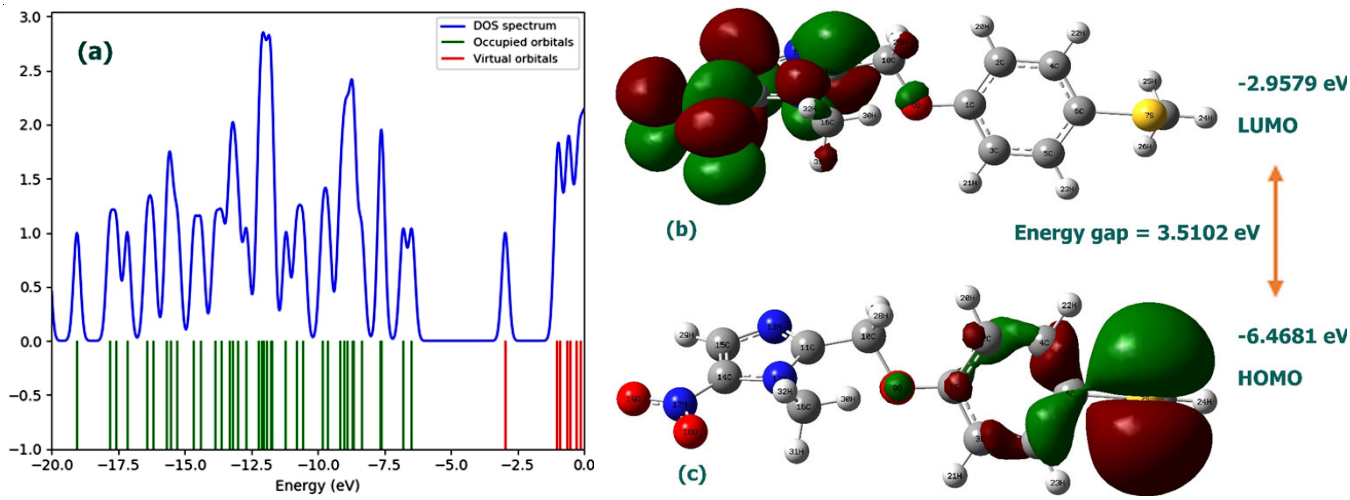

Fig. 4. DOS spectrum (a) LUMO (b) and HOMO (c) of fexinidazole

TABLE-5
THE ENTROPY (S), SPECIFIC HEAT CAPACITIES AT CONSTANT VOLUME (CV) AND PRESSURE (CP) OF FEXINIDAZOLE

Temp. (K)	S (a.u.)	CV (a.u.)	CP (a.u.)
100	92.080	30.393	32.380
200	115.639	48.063	50.050
300	136.663	66.429	68.416
400	156.853	84.172	86.159
500	176.236	99.440	101.428
600	194.611	111.908	113.895
700	211.885	122.008	123.995
800	228.073	130.271	132.258
900	243.241	137.120	139.107
1000	257.471	142.860	144.848

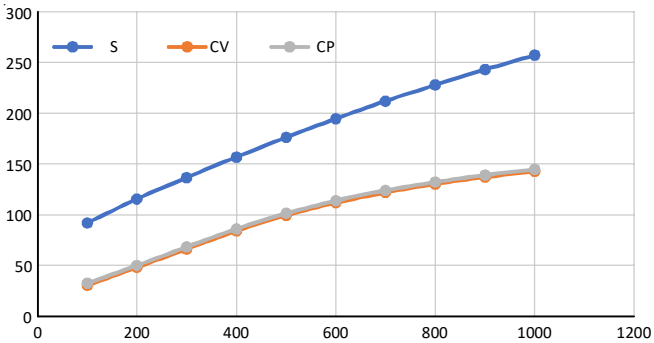

Fig. 5. The graphical representation of entropy (S), specific heat capacities at constant volume (CV) and pressure (CP) of fexinidazole

Non-linear optical activity: The movement of electron clouds from donor to acceptor, swift non-linear optical response times, low ionization constants and elevated laser affect levels are typically the primary factors contributing to non-linear the optical activity. Despite all these advantages, organic molecules have their flaws. For example, they tend to be heat unstable and relax to a random orientation quite easily [36]. When electromagnetic fields in various media interact, they alter the phase, frequency and amplitude of the incident fields and other propagation properties to generate new fields, a phenomenon known as a non-linear optical effect (NLO) [37]. Taylor's series expansion of the total dipole moment, which is independent of the field, can be used to illustrate the non-linear optical response of an isolated molecule in an electric field.

$$\mu_{tot} = \mu_0 + \alpha_{ij}E_j + \beta_{ijk}E_{jk} + ... \quad (2)$$

where μ_0 is the permanent dipole moment; α is the linear polarizability and β_{ijk} is the first hyperpolarizability tension component. Various parameters like μ, α, α_{tot}, β_{tot} and β_{vec} are examined in the gaseous phase and defined as follows:

$$\mu = \sqrt{\mu_x^2 + \mu_y^2 + \mu_z^2} \quad (3)$$

$$\alpha = \frac{\alpha_{xx} + \alpha_{yy} + \alpha_{zz}}{3} \quad (4)$$

$$\alpha_{tot} = \frac{1}{\sqrt{2}}\sqrt{(\alpha_{xx} - \alpha_{yy})^2 + (\alpha_{yy} - \alpha_{zz})^2 + (\alpha_{zz} - \alpha_{xx})^2 + 6\alpha_{xx}^2} \quad (5)$$

$$\beta_{Tot} = \sqrt{\beta_x^2 + \beta_y^2 + \beta_z^2} \quad (6)$$

where

$$\beta_x = \beta_{xxx} + \beta_{xyy} + \beta_{xzz} \quad (7)$$

$$\beta_y = \beta_{yyy} + \beta_{xxy} + \beta_{yzz} \quad (8)$$

$$\beta_z = \beta_{zzz} + \beta_{xxz} + \beta_{yyz} \quad (9)$$

$$\beta_{vec} = \frac{3}{5}\sqrt{(\beta_{xxx} + \beta_{xyy} + \beta_{xzz})^2 + (\beta_{yyy} + \beta_{xxy} + \beta_{yzz})^2 + (\beta_{zzz} + \beta_{xxz} + \beta_{xyz})^2} \quad (10)$$

The computed values have been converted into electrostatic units (esu) since the polarizabilities (α) and hyperpolarizability (β) of the Gaussian 16W output are provided in atomic units (a.u.) (α; 1 a.u. = 0.1482×10^{-24} esu, for β; 1 a.u = 8.6393×10^{-33} esu) [38]. The dipole moment, polarizability, α_{tot}, first-order hyperpolarizability and β_{vec} are calculated as 1.4778 Debye, 3.0586 e^{-23} esu, 1.0330 e^{-22} esu, 3.9611 e^{-30} esu and 2.3766 e^{-30} esu, respectively (Table-6). *para*-Nitroaniline (pNA) and urea were found to have first hyperpolarizability parameters of 15.5 $\times 10^{-24}$ and 0.13×10^{-24} esu, respectively [39,40]. This calculation indicates that the molecule exists in the first hyperpolarizability parameter about two times higher than in urea and pNA, respectively, by 231 times [41]. The high values may be due to the donor-acceptor system, such as -NO_2 and aromatic rings in the molecular system. The length of the bridge connecting the end groups of molecule may be another factor contributing to the high hyperpolarizability value. The non-linear optical features could be enhanced with an extended bridge connecting the donor and acceptor groups. The small HOMO-LUMO energy gap suggests its potential as a suitable candidate for NLO materials.

TABLE-6
THE STATIC DIPOLE MOMENT, STATIC FIRST ORDER HYPERPOLARIZABILITY AND STATIC POLARIZABILITY OF FEXINIDAZOLE

Dipole-moment (D)		Static first order hyperpolarizability (a.u.)	
μ_x	1.3753		
μ_y	0.3400	β_{xxx}	409.6348
μ_z	0.4206	β_{xxy}	-323.7797
μ (Debye)	1.4778	β_{xyy}	-121.9585
Static polarizability (a.u.)		β_{yyy}	5.1125
α_{xx}	303.0972	β_{xxz}	76.5441
α_{xy}	4.7373	β_{xyz}	-47.0571
α_{yy}	176.0666	β_{yyz}	-39.9531
α_{xz}	7.2291	β_{xzz}	59.2095
α_{yz}	3.1981	β_{yzz}	39.8298
α_{zz}	139.9940	β_{zzz}	73.6226
α (a.u.)	206.3859	β_{Tot} (a.u.)	458.5053
α (e.s.u)	30.0586×10^{-24}	β_{Tot} (e.s.u)	3.9611×10^{-30}
α_{tot} (a.u.)	697.086	β_{Vec} (a.u.)	275.1031
α_{tot} (e.s.u)	1.0330×10^{-22}	β_{Vec} (e.s.u.)	2.3766×10^{-30}

Non-covalent bond interaction: Mulitwfn 3.8 is the best tool to investigate all weak interactions inside a molecule. Most of the time, weak interactions between and within molecules keep molecules stable. In this work, the non-covalent interaction (NCI) approach was employed and the reduced density gradient (RDG) analysis to predict these interactions. To distinguish between bonded ($\lambda_2 < 0$) and non-bonded ($\lambda_2 > 0$) inter-

actions, the λ_2 sign is used [42]. For this case, the RDG scatter graph's λ_2 sign and ρ function from -0.05 to +0.50 a.u. The peaks above +0.2 a.u. are responsible for the effect of steric repulsion [43] in the ring. The van der Waals (vdW) forces (dipole-dipole interactions and London forces) are represented by the spikes that emerge in the $\lambda_2 = 0$ region [44]. The spikes in the $\rho > 0$ and $\lambda_2 < 0$ regions represent the electrostatic interactions like hydrogen and halogen bonds. It is evident from Fig. 6 that this molecule has steric repulsion and vdW forces. The vdW forces in the isosurface are depicted as greenish-brown circles (Fig. 6b), whereas a red dot inside the ring represents the steric repulsion forces.

Fukui Function analysis: A popular local density functional descriptor for chemical reactivity and site selectivity is the Fukui function [45]. The preferred areas where a chemical species will alter its density when the number of electrons fluctuates are indicated by local reactivity descriptors [46]. The related atomic or condensed Fukui function on the j^{th} atom can be defined as follows:

$$f_j^+ = Q_j(N+1) - Q_j(N) \quad (11)$$

$$f_j^- = Q_j(N) - Q_j(N-1) \quad (12)$$

$$f_j^0 = \frac{1}{2}[Q_j(N+1) - Q_j(N-1)] \quad (13)$$

The electrophilic, nucleophilic and free radical molecules are symbolized by the symbols, f_j^-, f_j^+, f_j^0 respectively. The atomic charge at the j^{th} atomic site is denoted by Q_j, which represents the chemical species that is neutral (N), anionic (N+1), or cationic (N-1) chemical species [47]. A dual descriptor Δf(r), defined as the difference between the nucleophilic and electrophilic Fukui function and provided by eqn. 14 and defined as follows [48]:

$$\Delta f(r) = \left[f_j^+ - f_j^-\right] \quad (14)$$

The location is more favourable for an electrophilic attack when the dual descriptor $\Delta f(r) < 0$ and more favourable for a nucleophilic attack when the dual descriptor $\Delta f(r) > 0$. The Dual descriptor Δf(r) provides a clear differentiation between electrophilic and nucleophilic assault at a certain site based on their sign.

Dual descriptor values for the investigated molecule is given in Table-7. Table-7 contains the cationic, anionic and neutral charges on the basis of Mulliken papulation and natural population analyses. According to Mulliken population analysis, the nucleophilic attack is possible at 6C (cationic – 1.0144 a.u.), anionic (1.3276 a.u.) and neutral (1.2615 a.u.) molecules. Nucleophilic attack is plausible at 17N (cationic – 0.7644 a.u.), anionic (0.7698 a.u.) and neutral (0.7892 a.u.) molecules, according to NPA. According to Mulliken population analysis, for cationic type, the electrophilic attack is in the order of 8C > 4C > 10C > 1C > 16C > 11C > 17N > 14C > 3C > 5C > 13N > 12N. The nucleophilic attack is in the order of 6C > 15C > 2C > 29H > 22H > 27H > 28H > 21H > 13N > 12N > 18O > 9O > 19O are the best areas for free radical attack. For an anionic radical, the order of electrophilic attack is 4C > 8C > 1C > 10C > 11C > 16C > 17N > 14C > 5C. For the same species, the nucleophilic attack order is 6C > 15C > 2C > 31H > 29H > 22H > 27H > 21H > 32H. The sites 19O, 13N, 12N and 9O will face free radical attacks.

Natural population study for cationic species indicates that the order of the electrophilic assault is of 13N > 16C > 18O > 19O > 3C > 9O > 2C > 8C. For the same species the anionic order is 17N > 1C > 11C > 10C > 21H > 31H > 32H. The electrophilic attack for anionic species is in the spectrum of 19O > 18O > 13N > 3C > 2C > 16C > 9O > 78S > 14C > 8C. For the same species, the nucleophilic attack is in the order of 17N > 1C > 10C > 12N > 21H > 20H > 31H. For neutral molecule, the assault by the electrophile is in the sequence of 13N > 3C > 16C > 19O > 18O > 90 > 2C > 7S and the nucleophilic attacks is in the order of 7S > 2C > 9O > 18O > 19O > 16C > 3C > 13N. In accordance with the dual descriptor criterion, the possible electrophilic sites in the tested molecules are 8C > 12N >10C > 4C > 5C > 16C > 1C > 6C since they are having negative values [$\Delta f(r) < 0$]. All other sites are more prone to nucleophilic attack since they have positive values [$\Delta f(r) > 0$]. The values are picturized in Fig. 7.

Natural bonding analysis: Natural bond analysis (NBO) examines the charge transfer within the molecule and the interactions between intermolecular bonds [49]. Stabilization energy $E^{(2)}$ is acquired by separating Lewis type NBO from non-Lewis-type NBOs. The stabilization energy was determined using eqn. 15 [50,51]:

$$E^{(2)} = \frac{-q_i \left|F^{ij}\right|^2}{\epsilon_j^{(NL)} - \epsilon_i^{(L)}} \quad (15)$$

where $\epsilon_j^{(NL)}$ denotes the non-Lewis NBO's energy $\epsilon_i^{(L)}$ is the Lewis NBO's energy and F^{ij} the off-diagonal NBO member of

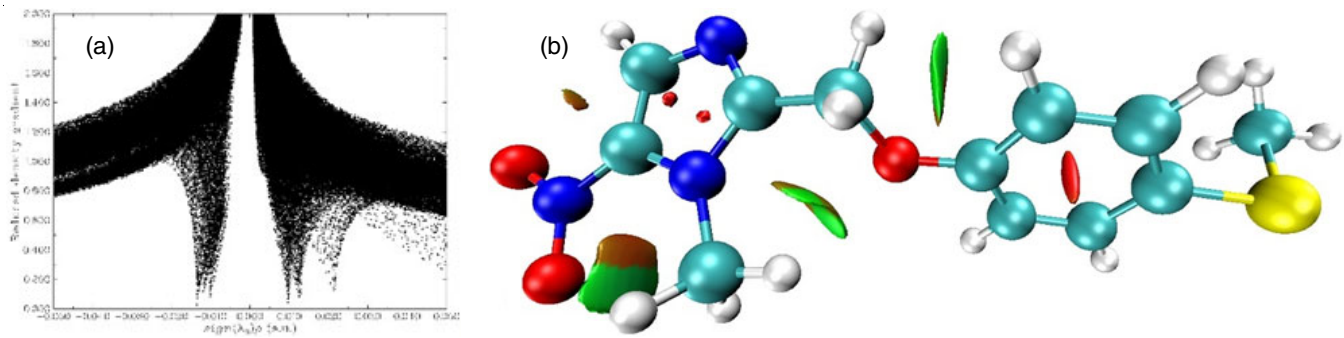

Fig. 6. Reduced density graph (RDG) and isosurface plots for fexinidazole

TABLE-7
MPA AND NPA VALUES FOR FEXINIDAZOLE

Atoms	MPA (a.u.)			NPA (a.u.)			
	$Q_{(N+1)}$	$Q_{(N0)}$	$Q_{(N-1)}$	f_j^+	f_j^-	f_j^0	Δf(r)
1C	-0.4244	-0.4596	-0.4301	0.5690	0.5830	0.5285	-0.014
2C	0.3563	0.3373	0.2993	-0.3123	-0.4649	-0.4258	0.1526
3C	-0.1899	-0.2470	-0.1971	-0.3784	-0.5019	-0.4716	0.1235
4C	-0.7302	-0.8724	-0.8501	-0.0493	-0.0139	0.0118	-0.0354
5C	-0.1546	-0.3223	-0.3071	0.0116	0.0429	0.0747	-0.0313
6C	1.0144	1.3276	1.2615	0.0468	0.0552	0.0149	-0.0084
7S	0.1532	-0.2429	-0.1470	0.0934	-0.3148	-0.2402	0.4082
8C	-0.7889	-0.6378	-0.7484	-0.2926	-0.1248	-0.2365	-0.1678
9O	0.0350	-0.0105	-0.0343	-0.3703	-0.4336	-0.4266	0.0633
10C	-0.4555	-0.4282	-0.4034	0.2635	0.3677	0.3526	-0.1042
11C	-0.4099	-0.4246	-0.4202	0.2806	0.0910	0.2042	0.1896
12N	-0.0038	-0.0330	-0.0113	0.1150	0.2414	0.1651	-0.1264
13N	-0.0080	-0.0870	-0.0355	-0.5273	-0.6195	-0.5427	0.0922
14C	-0.3083	-0.3237	-0.3447	-0.1179	-0.1936	-0.1693	0.0757
15C	0.6272	0.4639	0.6162	0.1789	0.0651	0.1467	0.1138
16C	-0.4185	-0.4097	-0.4221	-0.4558	-0.4344	-0.4683	-0.0214
17N	-0.3541	-0.4085	-0.3646	0.7644	0.7698	0.7892	-0.0054
18O	0.0257	-0.2043	-0.0031	-0.4136	-0.6760	-0.4552	0.2624
19O	0.0432	-0.1907	0.0043	-0.4111	-0.6926	-0.4644	0.2815
20H	0.2205	0.1757	0.1739	0.1901	0.1817	0.1762	0.0084
21H	0.2408	0.1852	0.1910	0.2184	0.1979	0.1994	0.0205
22H	0.2543	0.1922	0.2130	0.1527	0.0973	0.1082	0.0554
23H	0.2397	0.1707	0.1955	0.1525	0.0893	0.0959	0.0632
24H	0.2204	0.1018	0.1674	0.1987	0.0917	0.1541	0.107
25H	0.2268	0.1592	0.1802	0.1485	0.0610	0.0972	0.0875
26H	0.2208	0.1548	0.1791	0.1418	0.0573	0.0965	0.0845
27H	0.2495	0.1855	0.2161	0.0546	-0.0019	0.0213	0.0565
28H	0.2429	0.1591	0.2009	0.0218	-0.0615	-0.0268	0.0833
29H	0.2798	0.1993	0.2487	0.1554	0.1046	0.1398	0.0508
30H	0.1313	0.1081	0.1498	0.1510	0.1118	0.1576	0.0392
31H	0.2355	0.2004	0.2164	0.2099	0.1710	0.2027	0.0389
32H	0.2289	0.1813	0.2054	0.2098	0.1538	0.1908	0.056

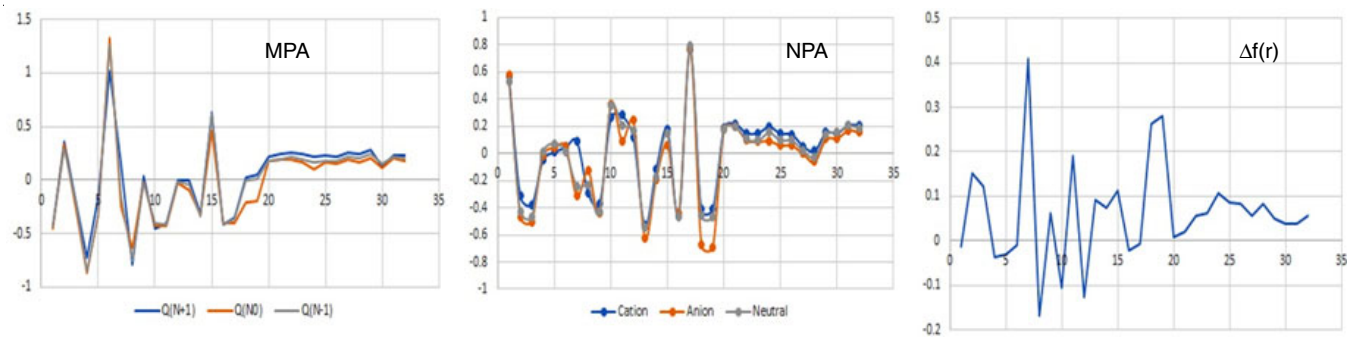

Fig. 7. A graphical representation of MPA, NPA and Δf(r) values of fexinidazole

the Fock matrix. The analysis of the specified chemical has been carried out using the same theoretical framework.

Table-8 contains the specified values for σ→σ*, σ→π*, π→LP, π→π*, LP→σ*, LP→π* transitions. Electron density transfer from the donor σ(N12-C16) to σ*(N17-O19) and σ(C16-H32) to σ*(N17-O18) resulted in a strong interaction with stabilization energies of 11.09 and 10.43 kcal/mol. With stabilization energies of 32.60, 17.02 and 14.13 kcal/mol, respectively, the delocalization of electrons is obtained from σ(C16-H32) to π*(N17-O19), σ(C16-H31) to π*(N17-O19) and σ(N12-C16) to π*(N17-O19). A π(N17-O19) interaction with stabilisation energy 11.41 kcal/mol to acceptor LP(3) O18.

From π(C4-C6) to π*(C3-C5), π(C3-C5) to π*(C4-C6), π(C1-C2) to π*(C4-C6) and π(C11-N13) to π*(C14-C15) electrons delocalize with high stabilization energies of 26.42, 23.02, 22.65 and 21.47 kcal/mol, respectively.

The moderate stabilization energies of 14.26, 10.50 and 10.47 kcal/mol respectively, is the result of electron donation from LP(2) O19, LP(2) O18 and LP(2) O19 to the antibonding σ*(N17-O18), σ*(C14-N17) and σ*(C14-N17) respectively.

TABLE-8
SECOND ORDER PERTURBATION THEORY ANALYSIS OF FOCK MATRIX NBO BASIS OF FEXINIDAZOLE

NBO No.	Type	Donor NBO	eD (a.u)	Type	Acceptor NBO	eD (a.u)	$E^{(2)a}$ (kcal/mol)	E(j)-E(i)[b]	F(i,j)[c]
3	π	C1 - C2	1.66785	π*	C3-C5	0.30271	15.91	0.30	0.062
4	π	C1 - C2	1.66785	π*	C4 - C6	0.36285	23.02	0.29	0.074
16	π	C3 - C5	1.69572	π*	C1 - C2	0.38764	16.88	0.27	0.072
17	π	C3 - C5	1.69572	π*	C4 - C6	0.36285	22.65	0.28	0.062
22	π	C4 - C6	1.69023	π*	C1 - C2	0.38764	16.25	0.28	0.061
23	π	C 4 - C 6	1.69023	π*	C 3 - C5	0.30271	21.47	0.29	0.071
34	σ	C11-N12	1.98226	σ*	C14 -N17	0.08780	4.98	1.18	0.070
38	π	C11 - N13	1.78554	?*	C14 -C15	0.35811	26.42	0.32	0.085
40	σ	N12 - C16	1.98938	σ*	N17-O18	0.05842	6.06	1.40	0.083
41	σ	N12 - C16	1.98938	σ*	N17- O19	0.05415	11.09	3.15	0.169
42	σ	N12 - C16	1.98938	π*	N17 - O19	0.66018	14.13	4.30	0.268
43	σ	N13 - C15	1.97632	σ*	C10 - C11	0.02725	6.00	1.19	0.076
44	σ	N13 - C15	1.97632	σ*	C14 - N17	0.08780	4.99	1.14	0.068
45	σ	C14 - C15	1.97911	σ*	N12 - C16	0.01968	5.36	1.04	0.067
46	π	C14 - C15	1.75391	π*	C11 - N13	0.40811	13.41	0.29	0.058
50	σ	C16 - H31	1.98561	π*	N17 - O19	0.66018	17.02	4.06	0.285
51	σ	C16 - H32	1.98637	σ*	N17 - O18	0.05842	10.43	1.16	0.099
52	σ	C16 - H32	1.98637	σ*	N17 - O19	0.05415	6.49	2.90	0.124
53	σ	C16 - H32	1.98637	π*	N17 - O19	0.66018	32.60	4.05	0.394
54	π	N17 - O19	1.98611	LP(3)	O18	1.47883	11.41	0.17	0.077
59	LP(2)	S7	1.93450	σ*	C4 - C6	0.02948	5.03	0.80	0.057
63	LP(1)	O9	1.96481	σ*	C1 - C2	0.02843	6.39	1.12	0.076
68	LP(2)	O9	1.85152	π*	C1 - C2	0.38764	27.85	0.35	0.094
69	LP(2)	O9	1.85152	σ*	C10 - H27	0.02080	5.31	0.70	0.056
70	LP(2)	O9	1.85152	σ*	C10 - H28	0.02718	5.43	0.71	0.057
71	LP(1)	N12	1.52733	π*	C11 - N13	0.40811	52.99	0.28	0.110
72	LP(1)	N12	1.52733	π*	C14 - C15	0.35811	32.24	0.28	0.088
78	LP(1)	N13	1.92662	σ*	C11 - N12	0.04559	8.41	0.83	0.075
86	LP(2)	O18	1.90004	σ*	C14 - N17	0.08780	10.50	0.64	0.073
89	LP(3)	O18	1.47883	π*	N17-O19	0.66018	5.19	3.80	0.130
93	LP(2)	O19	1.89355	σ*	C14 - N17	0.08780	10.47	0.63	0.073
94	LP(2)	O19	1.89355	σ*	N17 - O18	0.05842	14.26	0.92	0.103

[a]E(2) means energy of hyperconjugative interactions (stabilisation energy). eD/e means the electron density. [b]Energy difference between donor and acceptor i and j NBO orbitals. [c]F(i, j) is the Fock matrix element between i and j NBO orbital. LP(n)A is a valence lone pair orbital (n) on A atom.

LP(1) N12 to π*(C11-N13) and LP(1) N12 to π*(C14-C15) with stabilization energies of 52.99 and 32.24 kcal/mol, respectively. The most interaction energies in the molecule is due to resonance [50].

Hole-electron transfer analysis: The six lowest single excited states were calculated using time-dependent density functional theory (TD-DFT). The Io*p*(9/40 = 4) keyword is used in conjugation with the CAM-B3LYP method. The file .fch is created and examined. Table-9 lists all of the different outcomes that are obtained and Fig. 8 displays the hole-electron distribution, CDD function (charge density difference function), Sr function and C_{hole}-$C_{electron}$ function.

For all excitations, the Sr index values are greater than 0.5 a.u. (theoretical maximum limit is 1), indicating that around half of the hole and electron have matched exactly. The existence of a classic local type of excitation (LE) is confirmed by this prediction. For the compete excitation state, the Sr value is comparatively larger. In particular upto 0.8640 a.u. there is a significant excitation from S0→S6. The primary cause of this increased value is the presence of a extremely localized π-π*

TABLE-9
HOLE-ELECTRON INTERACTION PROPERTIES FOR FEXINIDAZOLE

Sm (a.u.)	Sr (a.u.)	D (Å)	H (Å)	τ (Å)	Excitation energy (eV)	Coulomb attractive energy (eV)	Δr (Å)	Λ
0.2582	0.5008	0.612	1.805	-0.605	3.978	7.8644	2.1505	0.4087
0.2827	0.5420	0.396	1.912	-0.903	4.466	7.6325	1.2086	0.4668
0.3728	0.6696	1.503	2.082	0.075	4.553	6.3195	3.0695	0.5443
0.0951	0.3044	6.271	2.716	3.909	5.011	2.9399	7.9799	0.0982
0.2816	0.5673	1.595	2.676	-0.633	5.078	5.3687	2.2680	0.4162
0.6115	0.8640	0.227	2.476	-1.683	5.159	5.9932	1.5115	0.5452

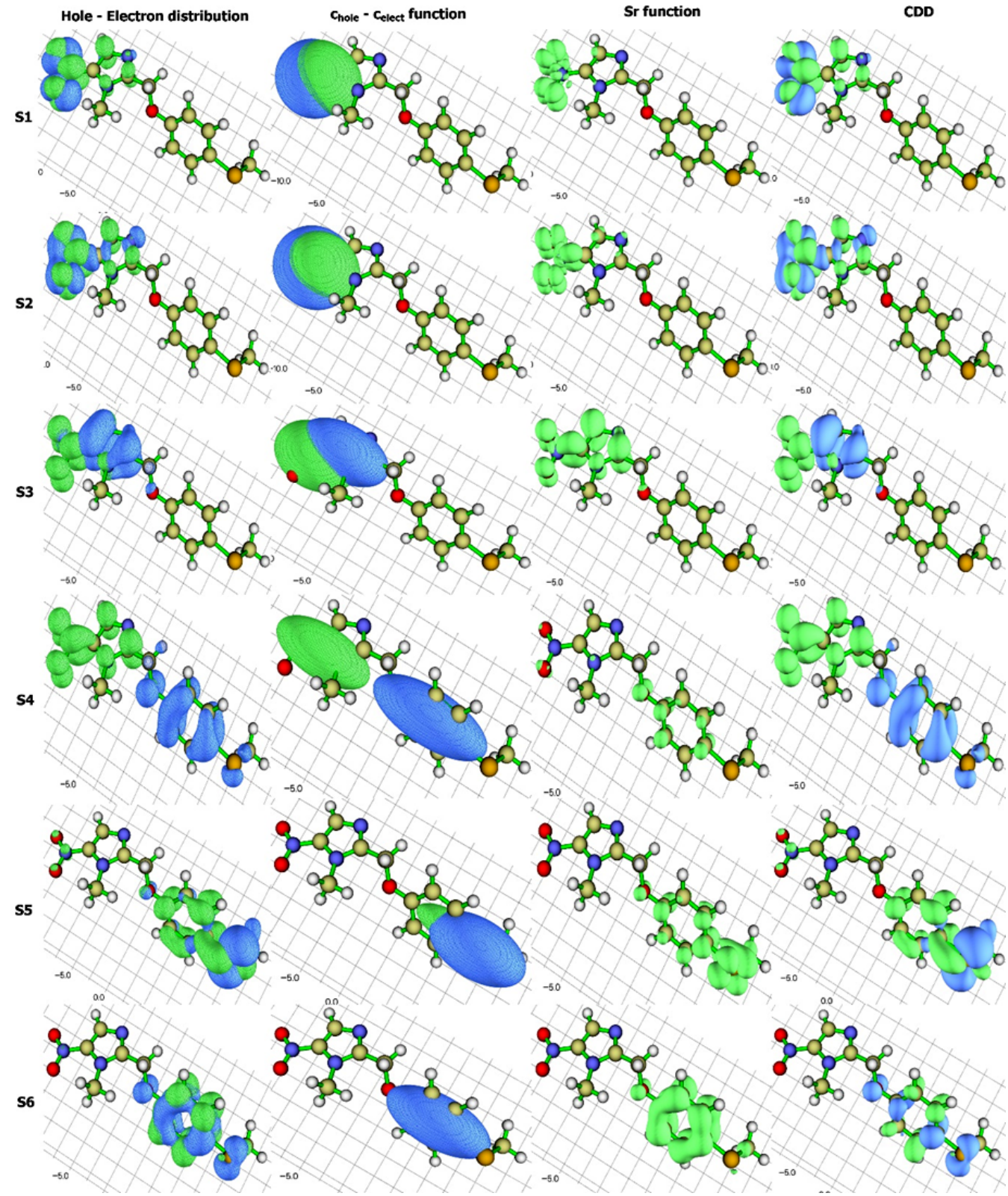

Fig. 8. A figure explaining hole-electron interaction in terms of (a) hole-electron distribution (b) Chole-Celect function (c) Sr function (d) CDD

type of excitation on the aromatic ring. There are only n-π* type excitations involved in the other excitations.

The normal circulation of holes and electrons is reflected in the H index's breadth. Information on the H index (for all excitations) is provided in Table-9, where it is found to be large. The H index is obviously bigger because the spreading of holes and electrons of S0→S4 is clearly wider (hole-electron distribution in S4).

The τ index values are negative except S0→S3 and S0→S4, meaning they are significantly less than zero, indicating that the deliveries of holes and electrons are not significantly separated. Furthermore, this confirms that there is no charge transfer (CT) type excitation for these excitations and only needs the existence of LE type excitation. The positive π indices for S0→S3 and S0→S4 indicate that they experience charge transfer (CT) excitation.

The electron-hole pair, the parameters of electron excitation are intimately associated with the Coulomb attractive energy. D index always has an impact on it. The greater the D index, the greater the separation between the primary electrons and holes distribution zones and thus, the lower the Coulomb attractive energy. The excitation S0→S4, has a higher D index value of 6.271 Å and the Columb attractive energy is determined to be 2.9399 eV which is the least. The fourth excited state (S0→S4) of a singlet system is typically the critical state to generate fluorescence, according to Kasha's rule and as such, it plays a crucial role in molecular photophysics [52].

Given that the Δr values are large, it is possible that the excitation from S0→S3 and S4 has a solid CT character. For other excitations the Δr values are too small (according to the creative article, the Δr value suggests using 2.0 Å as a standard to distinguish between CT and LE excitations). Only the CT excitation is followed by S0→S3 and →S4, whereas the other excitations adhere to the local excitation type (LE) because they have positive τ and high Δr values.

It is clearly apparent that the connection between the Lambda (Λ) and the Δr values is nearly inverse. The hole-electron separation distance decreases with increasing hole-electron overlapping area. In this case, the Λ value 0.0982, obtained for the excited state of S0→S4 is shorter than the other values. The following conclusions are drawn from the examination of Table-9 and the aforementioned isosurface maps (Fig. 8). S0 → S1, S2, S3, S4 and S5 follow n-π* transition while S0 → S6 follow π-π* transition. S0 → S3 and S4 follow CT type and S0 → S1, S2, S5, S6 follow LE type of excitation.

Heat map investigations: In order to see the nature of hole and electron in its lowest six excitation levels, heat maps are created for the studied molecule. Fig. 9 highlights the different fragmentation patterns. The calculated percentages of holes, electrons, overlap and the difference between them are displayed in Table-10. Fig. 10 illustrates the heat maps that were created for the lowest six excitations. It is observed that only the nitro group is present in large quantities of holes and electrons in the S0 → S1 and S2 excitations. For S0 → S3 excitation, percentage of holes are richer in fragment 4 and the percentage of electrons are richer in fragment 6. The fragment 2 has more percentage of holes and electrons for S0 → S6.

Study of inter-fragment charge transfer (IFCT): The inter-fragment charge transfer (IFCT) method based on the hole-electron analysis was also investigated. It offers a way to measure the charge transfer between distinct fragments for the S0→S3 and S6 transition states. Fig. 9 outlines the different fragment trends. Given that S0 → S3 and S6 exhibit positive τ values, the IFCT computation is performed for these two conditions.

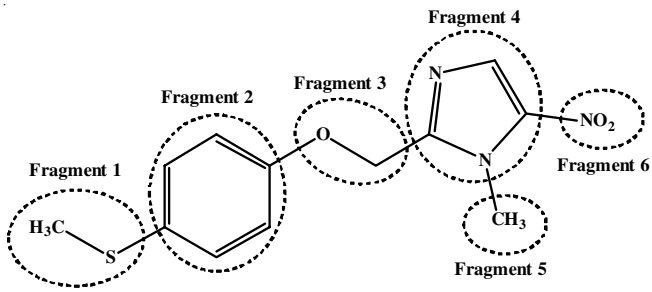

Fig. 9. Fragmentation trend for heat map and IFCT studies

TABLE-10
PARTICULARS ABOUT THE HEAT MAP GENERATION STUDY FOR FEXINIDAZOLE

Excitation	Fragments	Hole (%)	Electron (%)	Overlap (%)	Difference (%)
S1	1	0.03	0.26	0.09	0.23
	2	-0.14	0.39	0.00	0.53
	3	-0.10	0.54	0.00	0.64
	4	6.16	13.77	9.21	7.61
	5	-0.11	0.25	0.00	0.37
	6	94.16	84.78	89.35	-9.38
S2	1	0.15	0.26	0.19	0.11
	2	-0.21	0.28	0.00	0.50
	3	1.06	0.09	0.31	-0.97
	4	13.62	16.80	15.31	3.19
	5	0.15	0.26	0.20	0.11
	6	85.24	82.30	83.76	-2.94
S3	1	-0.08	-0.01	0.00	0.07
	2	0.97	0.82	0.90	-0.15
	3	1.03	0.82	0.92	-0.21
	4	89.12	25.70	47.86	-63.42
	5	0.47	0.60	0.53	0.13
	6	8.48	72.07	24.72	63.59
S4	1	8.68	-0.26	0.00	-8.94
	2	66.40	7.54	22.38	-58.86
	3	23.98	4.34	10.20	-19.64
	4	0.44	30.64	3.66	30.21
	5	0.20	1.01	0.45	0.81
	6	0.30	56.73	4.10	56.43
S5	1	84.99	40.88	58.94	-44.11
	2	12.80	54.78	26.48	41.98
	3	2.07	-1.52	0.00	-3.59
	4	0.12	3.52	0.65	3.40
	5	0.02	-0.32	0.00	-0.34
	6	-0.00	2.65	0.00	2.66
S6	1	15.41	5.30	9.03	-10.12
	2	74.38	92.59	82.99	18.21
	3	10.03	0.48	2.20	-9.55
	4	0.07	-0.65	0.00	-0.72
	5	0.10	0.69	0.27	0.59
	6	0.00	1.59	0.05	1.59

Table-11 illustrates the transfer between the many pieces. where the quantity of intra-fragment electron redistribution is indicated by the diagonal terms. Fraction 1 handovers 0.00655 electrons to fragment 2 and 0.00377 electrons to fragment 3 in S0 → S4. Additionally, 0.02661 electrons are transported from fragment 1 to fragment 4 and 0.04927 electrons are migrated to fragment 6. Consequently, in this excitation, charge transfer is plausible. The net transferred electrons between various fragments are presented in Table-12.

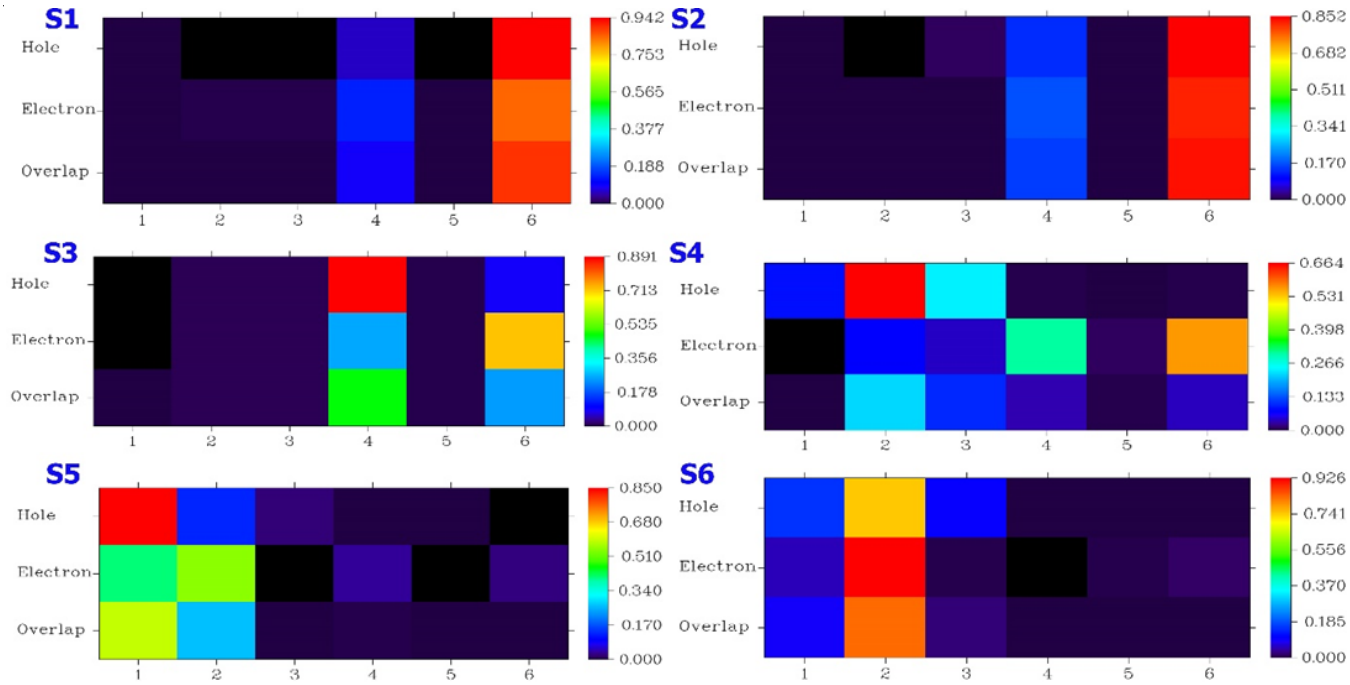

Fig. 10. Heat maps of fexinidazole (for lowest six excitations)

TABLE-11
TRANSFERRED ELECTRONS BETWEEN DIFFERENT FRAGMENTS

Excitation	Fragment	Fragment 1	Fragment 2	Fragment 3	Fragment 4	Fragment 5	Fragment 6 (NO_2)
S3	1	0.00000	0.00000	0.00000	0.00000	0.00000	0.00000
	2	0.00000	0.00008	0.00008	0.00250	0.00006	0.00702
	3	0.00000	0.00008	0.00008	0.00265	0.00006	0.00742
	4	0.00000	0.00734	0.00729	0.22907	0.00533	0.64230
	5	0.00000	0.00004	0.00004	0.00121	0.00003	0.00340
	6	0.00000	0.00070	0.00069	0.02180	0.00051	0.06112
S4	1	0.00000	0.00655	0.00377	0.02661	0.00087	0.04927
	2	0.00000	0.05009	0.02881	0.20347	0.00669	0.37669
	3	0.00000	0.01809	0.01040	0.07348	0.00242	0.13603
	4	0.00000	0.00033	0.00019	0.00134	0.00004	0.00247
	5	0.00000	0.00015	0.00009	0.00061	0.00002	0.00113
	6	0.00000	0.00022	0.00013	0.00091	0.00003	0.00168

Diagonal terms corresponds to amount of intra-fragment electron redistribution.

TABLE-12
NET TRANSFERRED ELECTRONS BETWEEN FRAGMENTS

Excitation	Fragment	Fragment 1	Fragment 2	Fragment 3	Fragment 4	Fragment 5	Fragment 6 (NO_2)
S3	1	–	0.00000	0.00000	0.00000	0.00000	0.00000
	2	–	–	-0.00001	-0.00484	0.00002	0.00632
	3	–	–	–	-0.00465	0.00002	0.00673
	4	–	–	–	–	0.00412	0.62050
	5	–	–	–	–	–	0.00289
	6	–	–	–	–	–	–
S4	1	–	0.00655	0.00377	0.02661	0.00087	0.04927
	2	–	–	0.01072	0.20314	0.00654	0.37646
	3	–	–	–	0.07329	0.00233	0.13591
	4	–	–	–	–	-0.00057	0.00156
	5	–	–	–	–	–	0.00110
	6	–	–	–	–	–	–

Determination of aromaticity: At the DFT/B3LYP/6-311++G(d,p) level of theory, the aromaticity of benzene ring in the title molecule was investigated and compared with that of toluene and benzene, which are also assessed at the same level of theory. The Multiwfn 3.8 tool yielded the results for the Para Delocalization Index (PDI) [53], BIRD aromaticity [54],

aromatic fluctuation index (FLU) [55], harmonic oscillator measure of aromaticity (HOMA) [56]. The following definitions apply to the FLU (eqn. 16), PDI (eqn. 17), HOMA (eqn. 18) and BIRD aromaticity (eqn. 19):

$$FLU = \frac{1}{n}\sum_{A-B}^{ring}\left[\left(\frac{V(B)}{V(A)}\right)^{\alpha}\left(\frac{\delta(A,B)-\delta_{ref}(A,B)}{\delta_{ref}(A,B)}\right)\right]^2 \quad (16)$$

where n is equal to the number of atoms in ring; δ_{ref} is the reference DI value, which is pre-calculated parameter; α is used to ensure the ratio of atomic valences is greater than one.

$$PDI = \frac{\delta(1,4)+\delta(2,5)+\delta(3,6)}{3} \quad (17)$$

$$HOMA = 1-\sum_{i}\frac{\alpha_{i,j}}{N}(R_{ref}-R_{i,j})^2 \quad (18)$$

where *N* is the total number of atoms considered; j denotes the atom next to atom i; α and R_{Ref} are the pre-calculated constants for each type of atomic pair.

$$I = 100[1-(\frac{V}{V_K})]$$

where

$$V = \frac{100}{\overline{N}}\sqrt{\frac{\sum_{i}(N_{i,j}-\overline{N})^2}{n}} \qquad N_{i,j} = \frac{a}{R_{i,j}}-b \quad (19)$$

where i cycles all of the bonds in ring; j denotes the atom next to atom i; n is the total number of bonds considered; N denotes Gordy bond order; N is the average value of N values; $R_{i,j}$ is bond length; a and b are predefined parameters respectively for each type of bonds; and V_K is pre-determined reference V.

The PDI, ELU, HOMA and BIRD aromaticity values are represented in Table-13. It clearly illustrated that fexinidazole has a lower value than toluene and benzene due to the substitution at the *para*-positions. A low FLU number indicates a higher aromatic nature. So the aromaticity is in the order of benzene > toluene > fexinidazole *i.e.* the aromaticity of the investigated molecule is marginally lower than that of the other two compounds. When HOMA is 1, it indicates that the ring is entirely aromatic because each bond's length is the same as the ideal value R_{Ref}. It is evident from Table-13 that toluene and benzene have higher aromaticities than fexinidazole. The order of PDI aromaticity is found to be benzene > toluene > fexinidazole.

TABLE-13
THE VARIOUS AROMATICITY VALUES DETERMINED FOR FEXINIDAZOLE, BENZENE AND TOLUENE

Molecule	PDI	HOMA	BIRD	FLU
Benzene	0.104540	0.988808	99.906373	0.000021
Toluene	0.101222	0.983513	97.877993	0.000738
Fexinidazole	0.090700	0.978302	95.906791	0.004300

Simulated STM image analysis: Utilizing the Multiwfn 3.8 tool, the simulated scanning tunneling microscope (STM) picture was generated and displayed in Fig. 11. It is an effective instrument for capturing the spatial fluctuations in the tunneling

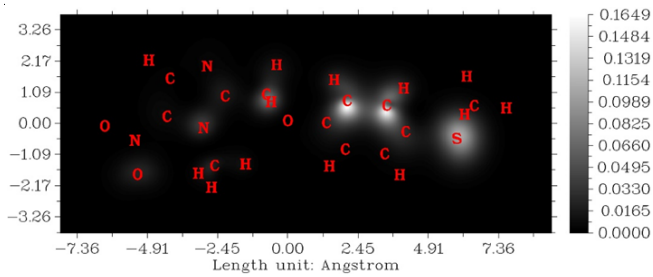

Fig. 11. STM image of fexinidazole

current at the interface between a sharp metallic tip and a conducting probe surface [57]. It is computed that the maximum value of the local density of states (LDOS) is 0.1649 a.u. at the bias voltage (V) is -5 V and the Z coordinate is 1.1 Å conditions. In this map, the tunnelling current (I) is stronger and the larger the LDOS, the brighter the white. The tunneling current (represented by I) and LDOS have a positive connection, in accordance with the Tersoff-Hamann model. It is evident that the 'I' signal is more pronounced at the two benzene ring carbon atoms and the sulphur atom that is joined to the aromatic ring.

Shaded surface map with a projection of LOL determination: Schmider & Becke [58,59] defined LOL (eqn. 20) as a function for finding extreme localization domains:

$$LOL(r) = \frac{\tau(r)}{1+\tau(r)} \quad (20)$$

where φi(r) are the Harttree-Fock of the Kohn-Sham orbitals and the dimensionless variable τ(r) is $g_0(r)/g(r)$ and is always reliant on positive one electron kinetic energy density.

The larger the LOL in a given location, the more likely it is that electron mobility will be constrained there. Fig. 12 shows the analysis of the shaded surface map using the localized locator (LOL) projection of fexinidazole. As may be observed, the surface represents a variety of colours. A strong electronic localization is represented by the orange and red colours. A depletion zone between the inner shell and the valence shell is represented by the blue colour circle [60]. The minimal values of the localized orbital locator are observed in the regions of hydrogen and carbon.

Molecular docking analysis

Preparation of protein: The 3D structure of the protein is obtained using 5UFG from the RCSB Protein Data Bank (http://www.rcsb.org). Using Discovery Studio Visualizer, the protein's heterocyclic atoms and water molecules were eliminated. The protein is then given hydrogen atoms before docking with the ligand. CHARMm algorithm was selected for forcefield application. Momany Rone algorithm was selected for partial charge analysis. For docking purpose, the protein is therefore processed and saved as a file in the .pdf format. The prepared protein was then analyzed for the quality in SAVES online tool (http://saves.mbi.ucla.edu). Upon examining the Ramachandran plot (Fig. 13) of the protein, it was found that each residue is within the expected range (91.3%).

Preparation of ligands: Chemsketch software creates the 2D structures of the drug molecule, fexinidazole and its derivatives, which are then saved as .mol files. The Avogadro tool

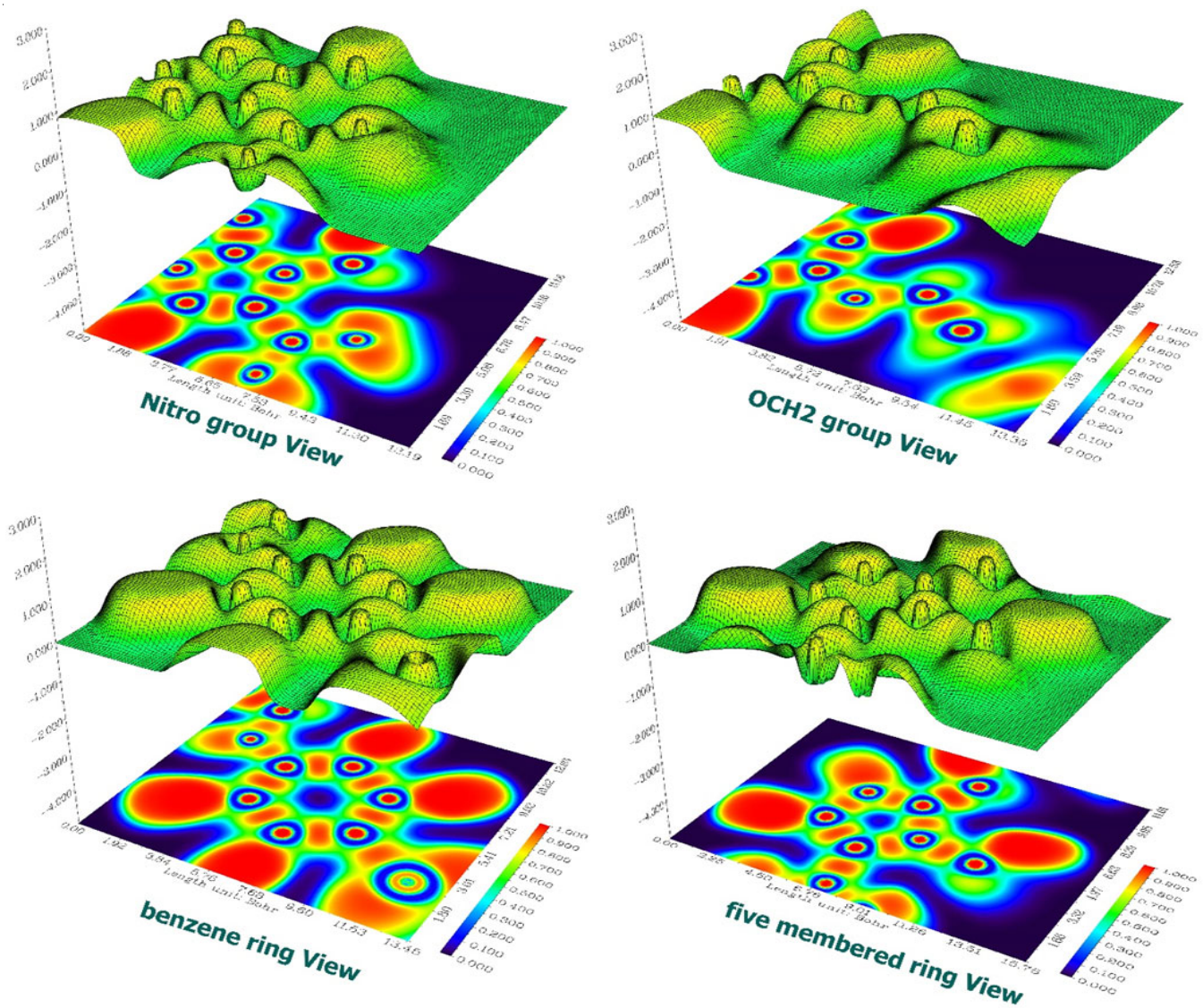

Fig. 12. The electron localization function (ELF) projection effect on a shaded surface map in the central QM structures of fexinidazole

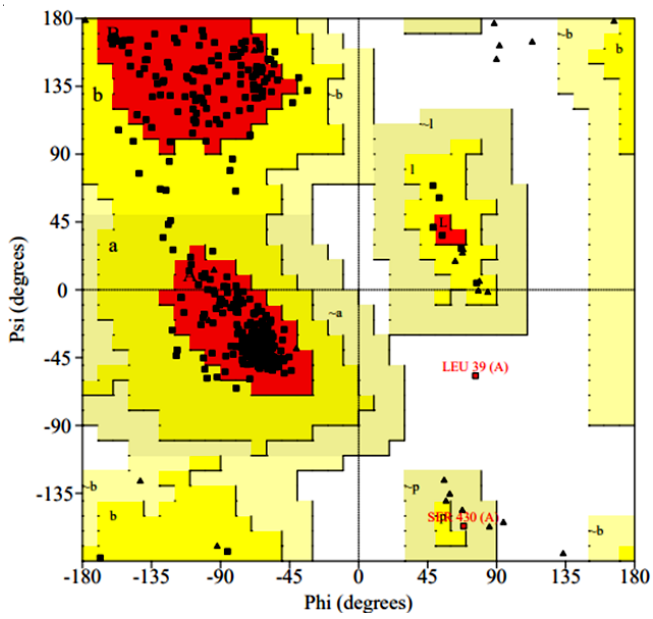

Fig. 13. Ramachandran plot for the prepared protein 5UFG

could then be used to subject individuals to the energy minimization method and the energy minimized molecules are saved in .pdb file format. MMFF94 is the force field which was used. The energy minimization process is a significant aspect prior to docking, since it reduces the computational time and yields accurate results. The 2D structures of the ligands and fexinidazole are shown in **Scheme-I**.

Docking studies: The prepared protein and prepared ligands were imported for docking using PyRx software (https://pyrx.sourceforge.io/). The size of the grid box was adjusted to 57.93 × 68.14 × 63.02 Å. Based on the docking scores (Table-14), fexinidazole has a docking value of -6.5 kcal/mol.

Structure activity relationship activity: For this, total 20 molecular structures were drawn from fexinidazole and subjected to docking. It is found that total 13 ligands can bind well with the protein 5UFG when compared with fexinidazole and the binding range is from -6.7 to -7.4 kcal/mol. The molecules 6 and 15 bind with the protein 5UFG with a score of -7.4 kcal/mol. So, these two molecules are selected for further investigations. The docking pattern of these molecules (fexinidazole

TABLE-14
DOCKING VALUES OF FEXINIDAZOLE AND ITS DERIVATIVES ALONG WITH XYZ ORIENTATION OF LIGANDS WITH PROTEIN

Molecule number	Functional groups	Pyrex binding values (kcal/mol)	Ligand docking orientation		
			X	Y	X
1	R^1-Br	-2.9	28.476909	11.002045	209.498274
2	R^1-CH_3	-2.8	28.636682	14.313909	206.796000
3	R^1-CHO	-7.0	31.396591	-16.598364	-10.758091
4	R^1-Cl	-6.9	31.561143	-16.336048	-11.303714
5	R^1-COOH	-5.9	10.666083	-2.315000	-5.345583
6	1-F	-7.4	27.354381	-13.947286	-12.532905
7	1-NH_2	-7.2	32.419435	-14.719087	-17.199913
8	1-NO_2	-7.2	31.942957	-13.166609	-16.135783
9	1-OCH_3	-7.3	32.595137	-14.829591	-17.076409
10	1-OH	-7.2	32.210545	-14.810636	-17.010000
11	2-Br	-5.9	44.990952	-0.744333	-3.852238
12	2-CH_3	-6.0	45.006524	-0.918286	-3.333000
13	2-CHO	-6.9	31.528864	-16.584136	-10.753182
14	2-Cl	-6.7	29.274333	-15.634905	-14.304952
15	2-COOH	-7.4	31.938959	-14.402458	-16.394750
16	2-F	-7.2	27.475905	-14.027524	-12.633286
17	2-NH_2	-6.9	30.999652	-13.644435	-15.302304
18	2-NO_2	-6.3	32.696913	-15.557913	-11.445783
19	2-OCH_3	-6.8	31.719818	-16.486818	-10.896682
20	2-OH	-6.1	31.944500	-16.847273	-10.872318
21	Fexinidazole	-6.5	30.686100	-15.394400	-12.482700

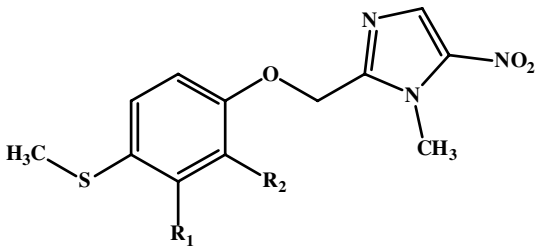

Molecule	R_1	R_2	Molecule	R_1	R_2
1	**-Br**	**-H**	**11**	**-H**	**-Br**
2	**-CH_3**	**-H**	**12**	**-H**	**-CH_3**
3	**-CHO**	**-H**	**13**	**-H**	**-CHO**
4	**-Cl**	**-H**	**14**	**-H**	**-Cl**
5	**-COOH**	**-H**	**15**	**-H**	**-COOH**
6	**-F**	**-H**	**16**	**-H**	**-F**
7	**-NH_2**	**-H**	**17**	**-H**	**-NH_2**
8	**-NO_2**	**-H**	**18**	**-H**	**-NO_2**
9	**-OCH_3**	**-H**	**19**	**-H**	**-OCH_3**
10	**-OH**	**-H**	**20**	**-H**	**-OH**
			21 (fexinidazole)	**-H**	**-H**

Scheme-I: The various structures of fexinidazole and its derivatives for the SAR investigations

and molecules 6 and 15) were analyzed with discovery studio Visualizer and shown in Fig. 14. Table-15 demonstrates the hydrogen bond distances and molecular docking results for the 5UFG protein and the best docking molecules (6 and 15).

Biological activity prediction

Drug likeness property: The biological activity and best binding of fexinidazole and other molecules (6 and 15) were also examined based on Lipinski's five rules (Ro5) [61]. The preADMET web server was used to acquire the drug score factors [62]. The (Milog P) partition coefficient of the active compound is found to be 2.27, suggesting that fexinidazole is soluble in biological milieu due to its lipophilicity. With the molecular weight of 279.32 g/mol, the fexinidazole molecule compiles with Lipinski's rule of five (Table-16). There are five rotatable bonds in the fexinidazole molecule, exemplifying the conformational flexibility. Table-17 describes the values for GPCR ligand (-0.51), ion channel modulator (-0.45), kinase inhibitor (-0.41), nuclear receptor ligand (-0.68), protease inhibitor (-0.73) and enzyme inhibitor (-0.23). The values of the other two derived molecule (6 and 15) are also shown in Tables 16 and 17 and also show the good similar results as compare to fexinidazole.

ADMET properties: The ADMET capabilities of fexinidazole are shown in Table-18. The gastrointestinal absorption is found to be very high but the BBB value is very low. This property is shown in Boiled Egg model (Fig. 15), which indicate that the permeability of fexinidazole in human skin is -6.23 cm/s meaning that it cannot be absorbed *via* the skin. There is no infringement and everything is following the regulations, as demonstrated by the rules of Lipinski, Ghose, Veber, Egan and Muegge. According to Swiss ADME, this is a lead like molecule since it has good lead-likeness. The other two molecules (molecules 6 and 15) also show similar types of values. Since, the best docking molecules (6 and 15) show good properties than fexinidazole, these molecules may be considered further for future research.

Conclusion

Fexinidazole is administered to treat sleeping sickness in South Africa. Gaussian 16W was utilized for the computation of all the physical characteristics. The B3LYP/6-311++G(d,p) level of theory has been selected. The absence of negative frequencies indicates that the molecule has undergone thorough optimization and achieved complete convergence. Mulliken's

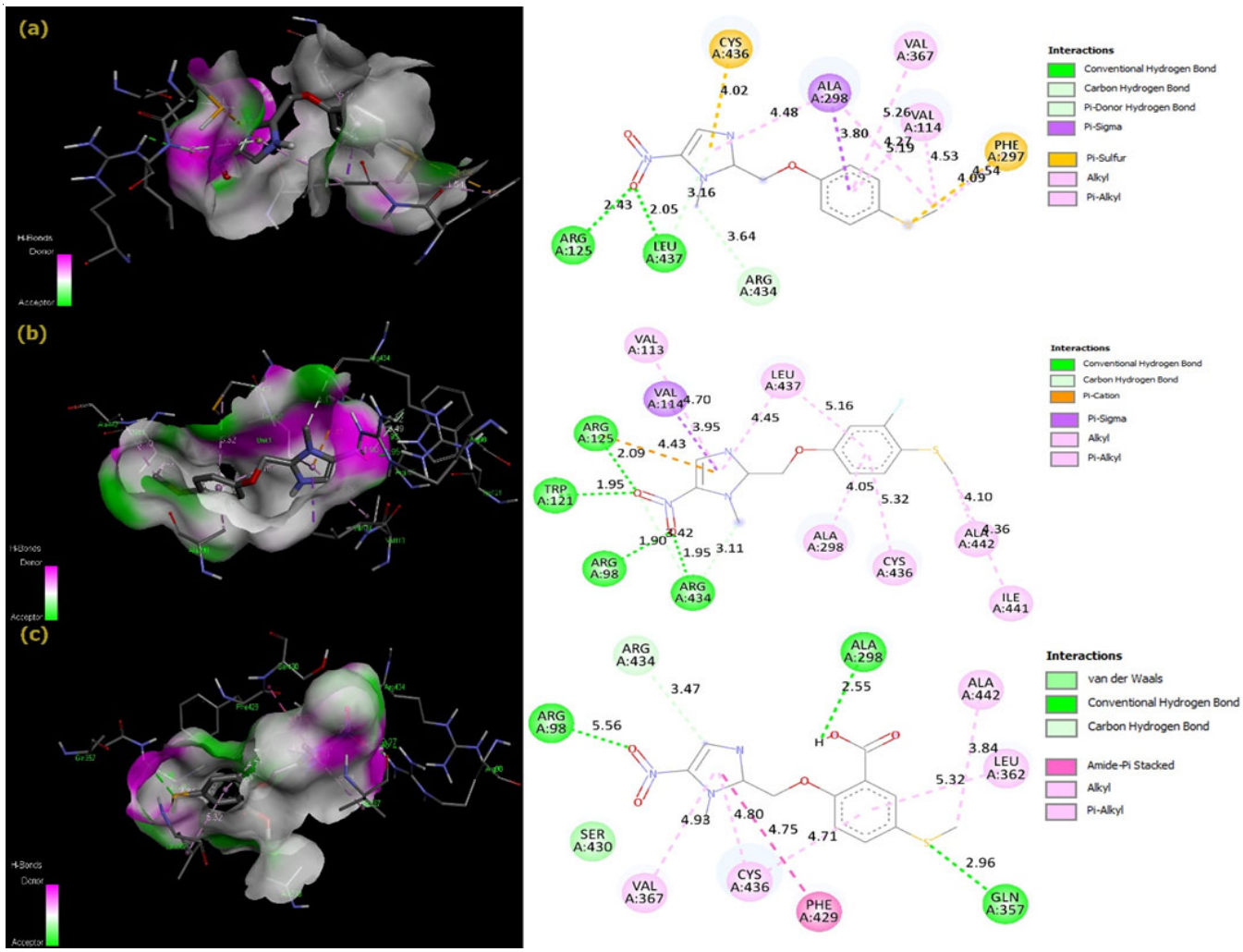

Fig. 14. 3D and 2D docking pattern of (a) fexinidazole (b) molecule 6 and (c) molecule 15

TABLE-15
DOCKING RESULTS AND INTERACTING AMINO ACIDS WITH HYDROGEN BOND DISTANCES

Molecule No.	Amino acid residue	Bonded atoms of ligands	Hydrogen bond distance (Å)	Number of hydrogen bond interaction
Molecule 21 (Fexinidazole)	ARG A:125	O	2.43	2
	LEU A:437	O	2.05	
Molecule 6	ARG A:125	O	2.09	4
	TRP A:121	O	1.95	
	ARG A:98	O	1.90	
	ARG A:434	O	1.95	
Molecule 15	ARG A:98	O	5.56	3
	ALA A:298	H	2.55	
	GLN A:357	S	2.96	

TABLE-16
DRUG-LIKENESS DESCRIPTOR OF FEXINIDAZOLE AND OTHER TWO BEST BINDING MOLECULES PREDICTED FROM MOLINSPIRATION

Descriptors	Fexinidazole	Molecule 6	Molecule 15
Hydrogen bond donors (HBD)	0	0	1
Hydrogen bond acceptors (HBA)	4	5	6
Partition coefficient (MilogP)	2.27	2.36	2.19
Molecular weight (MW)	279.32	297.31	323.33
Topological polar surface area (TPSA) (Å^2)	72.88	72.88	110.18
Number of atoms	19	20	22
Number of rotatable bonds	5	5	6
Number of violations	0	0	0

TABLE-17
BIOACTIVITY SCORE OF FEXINIDAZOLE AND ITS DERIVATIVES PREDICTED FROM MOLEINSPIRATION

Descriptors	Fexinidazole	Molecule 6	Molecule 15
GPCR ligand	-0.51	-0.37	-0.31
Ion channel modulator	-0.45	-0.56	-0.43
Kinase inhibitor	-0.41	-0.29	-0.34
Nuclear receptor ligand	-0.68	-0.65	-0.34
Protease inhibitor	-0.73	-0.71	-0.47
Enzyme inhibitor	-0.23	-0.28	-0.12

TABLE-18
PREDICTION OF ADMET PROFILES FOR FEXINIDAZOLE MOLECULE AND ITS DERIVATIVES

Descriptors	Fexinidazole	Molecule 6	Molecule 15
GI absorption	High	High	High
BBB permeant	No	No	No
P-gp substrate	No	No	No
CYP1A2 inhibitor	Yes	Yes	Yes
CYP2C19 inhibitor	Yes	Yes	Yes
CYP2C9 inhibitor	No	No	No
CYP2D6 inhibitor	No	No	No
CYP3A4 inhibitor	No	No	No
Log K_p (skin permeation)	-6.23 cm/s	-6.27 cm/s	-6.83 cm/s
Lipinski	Yes	Yes	Yes
Ghose	Yes	Yes	Yes
Veber	Yes	Yes	Yes
Egan	Yes	Yes	No (1 violation)
Muegge	Yes	Yes	Yes
Bioavailability score	0.55	0.55	0.56
PAINS	0 alert	0 alert	0 alert
Brenk	2 alerts	2 alerts	2 alerts
Leadlikeness	Yes	Yes	Yes
Synthetic accessibility	2.64	2.69	2.73

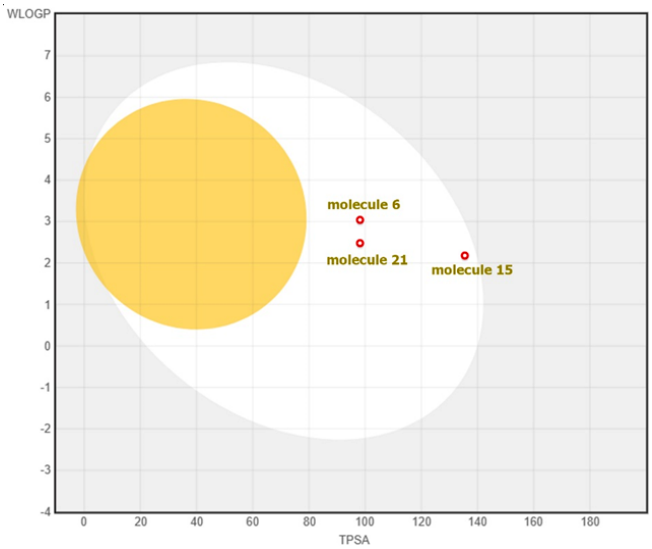

Fig. 15. Boiled Egg model for gastrointestinal absorption (GI) and brain penetration

investigation elucidates that carbon atom 6C possesses a significantly elevated positive charge, while carbon atom 4C exhibits the least substantial atomic charge. Electrophilic assault can occur at the oxygen atoms within the nitro group. Because of its narrow HOMO-LUMO energy gap, it can effectively function as an electron donor. The study on non-linear optics (NLO) elucidates that this particular molecule exhibits promising characteristics as a candidate for NLO applications. The molecule contains weak Van der Waals and steric repulsion forces. According to NPA analysis, there are possible attacks for electrophilic, nucleophilic and free radicals. The NBO studies are carried out to investigate about the stability. Hole-electron transfer analysis reveals that S0→S3 and S4 undergo CT type of excitation. The heat map, IFCT, STM and aromaticity experiments were also obtained and discussed. The structure activity relationship (SAR) activity is performed with 5UFG protein and two lead molecules are identified.

ACKNOWLEDGEMENTS

The authors thank the authorities of St. John's College for supplying computers and software facilities.

CONFLICT OF INTEREST

The authors declare that there is no conflict of interests regarding the publication of this article.

REFERENCES

1. D. Malvy and F. Chappuis, *Clin. Microbiol. Infect.*, **17**, 986 (2011); https://doi.org/10.1111/j.1469-0691.2011.03536.x
2. P.P. Simarro, A. Diarra, J.A. Ruiz Postigo, J.R. Franco and J.G. Jannin, *PLoS Negl. Trop. Dis.*, **5**, e1007 (2011); https://doi.org/10.1371/journal.pntd.0001007
3. M. Balasegaram, S. Balasegaram, D. Malvy and P. Millet, *PLoS Negl. Trop. Dis.*, **2**, e234 (2008); https://doi.org/10.1371/journal.pntd.0000234
4. F.A.S. Kuzoe, *Acta Trop.*, **54**, 153 (1993); https://doi.org/10.1016/0001-706X(93)90089-T
5. D.H. Molyneux, *Trans. R. Soc. Trop. Med. Hyg.*, **95**, 233 (2001); https://doi.org/10.1016/S0035-9203(01)90220-2
6. G. Hide, *Clin. Microbiol. Rev.*, **12**, 112 (1999); https://doi.org/10.1128/CMR.12.1.112
7. F. Torrico, J. Gascón, L. Ortiz, J. Pinto, G. Rojas, A. Palacios, F. Barreira, B. Blum, A.G. Schijman, M. Vaillant, N. Strub-Wourgaft, M.J. Pinazo, G. Bilbe and I. Ribeiro, *Clin. Infect. Dis.*, **76**, e1186 (2023); https://doi.org/10.1093/cid/ciac579
8. E.D. Deeks, *Drugs*, **79**, 215 (2019); https://doi.org/10.1007/s40265-019-1051-6
9. Fexinidazole: FDA-Approved Drugs, U.S. Food and Drug Administration. (Retrieved 16 July 2021).
10. N. Kerru, L. Gummidi, S.V.H.S. Bhaskaruni, S.N. Maddila, P. Singh and S.B. Jonnalagadda, *Sci. Rep.*, **9**, 19280 (2019); https://doi.org/10.1038/s41598-019-55793-5
11. N.D. Yilmazer and M. Korth, *J. Phys. Chem. B*, **117**, 8075 (2013); https://doi.org/10.1021/jp402719k
12. C. Faber, P. Boulanger, C. Attaccalite, I. Duchemin and X. Blase, *Phil. Trans. R. Soc., A:*, **372**, 0271 (2013); https://doi.org/10.1098/rsta.2013.0271
13. ACD/Chemsketch, 2017.2.1, Advanced Chemistry Development, Inc. (ACD/Labs), oronto, ON, Canada; www.acdlabs.com
14. M.D. Hanwell, D.E. Curtis, D.C. Lonie, T. Vandermeersch, E. Zurek and G.R. Hutchison, *J. Cheminform.*, **4**, 17 (2012); https://doi.org/10.1186/1758-2946-4-17
15. M.J. Frisch, G.W. Trucks, H.B. Schlegel, G.E. Scuseria, M.A. Robb, J.R. Cheeseman, G. Scalmani, V. Barone, G.A. Peterson, H. Nakatsuji, X. Li, M. Caricato, A.V. Marenich, J. Bloino, B.G. Janesko, R.Comperts, B. Mennucci, H.P. Hratchian, J.V.Oritz, A.F. Izmaylov, J.L. Sonnenberg, D. Williams-Young, F. Ding, F. Lipparini, F.Egidi, J. Goings, B. Peng, A. Petrone, T. Henderson, D. Ranasinghe, V.G. Zakrzewski, J. Gao, N.

Rega, G. Zheng, W. Liang, M. Hada, M. Ehara, K. Toyota, R. Fukuda, J. Hasegawa, M. Ishida, T. Nakajima, Y. Honda, O. Kitao, H. Nakai, T. Vereven, K. throssell, J.A. Montgomery, Jr., J.E. Peralta, F. Ogliaro, M.J. Bearpark, J.J. Heyd, E.N. Borhters, K.N. Kudin, V.N. Staroverov, T.A. Keith, R. Kobayashi, J. Normand, K. Raghavachari, A.P. Rendell, J.C. Burant, S.S. Iyengar, J. Tomasi, M. Cossi, J.M. Millam. M. Klene, C. Adamo, R. Cammi, J.W. Ochterski, R.L. Martin, K. Morokuma, O. Farkas, J.B. Forseman and D.J. Fox, Gaussian 16, Revision B.01, Gaussian, Inc., Wallingford CT (2016).
16. R. Dennington, T.A. Keith and J.M. Millam, GaussView, Version 6, Semichem Inc., Shawnee Mission, K.S. (2016).
17. A.D. Becke, *J. Chem. Phys.*, **98**, 5648 (1993); https://doi.org/10.1063/1.464913
18. C. Lee, W.X. Yang and R.G. Parr, *Phys. Rev. B Condens. Matter*, **37**, 785 (1988); https://doi.org/10.1103/PhysRevB.37.785
19. N. Singla and P. Chowdhury, *J. Mol. Struct.*, **1045**, 72 (2013); https://doi.org/10.1016/j.molstruc.2013.04.015
20. N.M. O'Boyle, A.L. Tenderholt and K.M. Langner, *J. Comput. Chem.*, **29**, 839 (2008); https://doi.org/10.1002/jcc.20823
21. T. Lu and F. Chen, *J. Comput. Chem.*, **33**, 580 (2012); https://doi.org/10.1002/jcc.22885
22. T. Lu and Q. Chen, *Comput. Theor. Chem.*, **1200**, 113249 (2021); https://doi.org/10.1016/j.comptc.2021.113249
23. W. Humphrey, A. Dalke and K. Schulten, *J. Mol. Graph.*, **14**, 33 (1996); https://doi.org/10.1016/0263-7855(96)00018-5
24. S. Dallakyan and A.J. Olson, *Methods Mol. Biol.*, **1263**, 243 (2015); https://doi.org/10.1007/978-1-4939-2269-7_19
25. T. Sasitha and W.J. John, *Heliyon*, **7**, e06127 (2021); https://doi.org/10.1016/j.heliyon.2021.e06127
26. Y. Diao, W.Y. Wang, Z.H. Wei and J.L. Wang, *Acta Crystallogr. Sect. E Struct. Rep. Online*, **67**, o3072 (2011); https://doi.org/10.1107/S1600536811041705
27. A.I. Aranburu Leiva, S.L. Benjamin, S.K. Langley and R.E. Mewis, *Acta Crystallogr. E Crystallogr. Commun.*, **72**, 1614 (2016); https://doi.org/10.1107/S2056989016016753
28. A. Schmidt, I. Jourdain, M. Knorr and C. Strohmann, *Acta Crystallogr. E Crystallogr. Commun.*, **79**, 516 (2023); https://doi.org/10.1107/S2056989023003717
29. H. El-Ouafy, M. Aamor, M. Oubenali, M. Mbarki, A.E. Haimouti and T. El-Ouafy, *Sci. Technol Asia*, **27**, 9 (2022).
30. R. Rahmani, N. Boukabcha, A. Chouaih, F. Hamzaoui and S. Goumri-Said, *J. Mol. Struct.*, **1155**, 484 (2018); https://doi.org/10.1016/j.molstruc.2017.11.033
31. S. Jeyavijayan, *Spectrochim. Acta A Mol. Biomol. Spectrosc.*, **136**, 890 (2015); https://doi.org/10.1016/j.saa.2014.09.110
32. T.H.M. Nayaka, I. Pushpavathi, Pavithra and Y.R. Nagesh, *Russ. J. Bioorg. Chem.*, **50**, 211 (2024); https://doi.org/10.1134/S1068162024010229
33. S. Saravanan and V. Balachandran, *Spectrochim. Acta A Mol. Biomol. Spectrosc.*, **138**, 406 (2015); https://doi.org/10.1016/j.saa.2014.11.091
34. G. Kanimozhi, S. Tamilselvan, A. Saral, S. Kaleeswaran, E. Geetha, A. Manikandan and S. Muthu, *Chem. Phys. Impact*, **8**, 100539 (2024); https://doi.org/10.1016/j.chphi.2024.100539
35. M. Ragamathunnisa, M. Revathi and M.J.V. Rani, *J. Adv. Appl. Sci. Res.*, **1**, 1 (2015).
36. R. Rajkumar, A. Kamaraj, S. Bharanidharan, H. Saleem and K. Krishnasamy, *J. Mol. Struct.*, **1084**, 74 (2015); https://doi.org/10.1016/j.molstruc.2014.10.035
37. H. Moghanian, A. Mobinikhaledi and R. Monjezi, *J. Mol. Struct.*, **1052**, 135 (2013); https://doi.org/10.1016/j.molstruc.2013.08.043
38. B. Rajasekhar, P.K. Muhammad Hijaz and T. Swu, *J. Mol. Struct.*, **1168**, 212 (2018); https://doi.org/10.1016/j.molstruc.2018.04.090
39. L.T. Cheng, W. Tam, S.H. Stevenson, G.R. Meredith, G. Rikken and S.R. Marder, *J. Phys. Chem.*, **95**, 10631 (1991); https://doi.org/10.1021/j100179a026
40. P. Kaatz, E.A. Donley and D.P. Shelton, *J. Chem. Phys.*, **108**, 849 (1998); https://doi.org/10.1063/1.475448
41. C. Adant, M. Dupuis and J.L. Bredas, *Int. J. Quantum Chem.*, **56(S29)**, 497 (1995); https://doi.org/10.1002/qua.560560853
42. A. Sagaama, N. Issaoui, O. Al-Dossary, A.S. Kazachenko and M.J. Wojcik, *J. King Saud Univ. Sci.*, **33**, 101606 (2021); https://doi.org/10.1016/j.jksus.2021.101606
43. Z. Jia, H. Pang, H. Li and X. Wang, *Theor. Chem. Acc.*, **138**, 113 (2019); https://doi.org/10.1007/s00214-019-2502-6
44. S. Khan, H. Sajid, K. Ayub and T. Mahmood, *J. Mol. Liq.*, **316**, 113860 (2020); https://doi.org/10.1016/j.molliq.2020.113860
45. M.L. Beatrice, S.M. Delphine, M. Amalanathan, M.S.M. Mary, H.M. Robert and K.T. Mol, *J. Mol. Struct.*, **1238**, 130381 (2021); https://doi.org/10.1016/j.molstruc.2021.130381
46. R.R. Pillai, V.V. Menon, Y.S. Mary, S. Armakovic, S.J. Armakovic and C.Y. Panicker, *J. Mol. Struct.*, **1130**, 208 (2017); https://doi.org/10.1016/j.molstruc.2016.10.032
47. P.K. Chattaraj, B. Maiti and U. Sarkar, *J. Phys. Chem. A*, **107**, 4973 (2003); https://doi.org/10.1021/jp034707u
48. C. Morell, A. Grand and A. Toro-Labbé, *J. Phys. Chem. A*, **109**, 205 (2005); https://doi.org/10.1021/jp046577a
49. C. James, A.A. Raj, R. Reghunathan, V.S. Jayakumar and I.H. Joe, *J. Raman Spectrosc.*, **37**, 1381 (2006); https://doi.org/10.1002/jrs.1554
50. E.S. Ashlin, G.E. Sheela and P.R. Babila, *Chem. Phys. Impact*, **6**, 100186 (2023); https://doi.org/10.1016/j.chphi.2023.100186
51. R. Kumar, A. Kumar, V. Deval, A. Gupta, P. Tandon, P.S. Patil, P. Deshmukh, D. Chaturvedi and J.G. Watve, *J. Mol. Struct.*, **1129**, 292 (2017); https://doi.org/10.1016/j.molstruc.2016.09.087
52. Z. Liu, T. Lu and Q. Chen, *Carbon*, **165**, 461 (2020); https://doi.org/10.1016/j.carbon.2020.05.023
53. J. Poater, M. Duran, M. Solà and B. Silvi, *Chem. Rev.*, **105**, 3911 (2005); https://doi.org/10.1021/cr030085x
54. C.W. Bird, *Tetrahedron*, **41**, 1409 (1985); https://doi.org/10.1016/S0040-4020(01)96543-3
55. E. Matito, M. Duran and M. Solà, *J. Chem. Phys.*, **122**, 014109 (2005); https://doi.org/10.1063/1.1824895
56. T.M. Krygowski, *J. Chem. Inf. Comput. Sci.*, **33**, 70 (1993); https://doi.org/10.1021/ci00011a011
57. B. Donner, M. Kleber, C. Bracher and H.J. Kreuzer, *Am. J. Phys.*, **73**, 690 (2005); https://doi.org/10.1119/1.1930867
58. H.L. Schmider and A.D. Becke, *J. Mol. Struct. THEOCHEM*, **527**, 51 (2000); https://doi.org/10.1016/S0166-1280(00)00477-2
59. M.R. Bozorgmehr, J. Chamani and G. Moslehi, *J. Biomol. Struct. Dyn.*, **33**, 1669 (2015); https://doi.org/10.1080/07391102.2014.967299
60. O. Noureddine, N. Issaoui, M. Medimagh, O. Al-Dossary and H. Marouani, *J. King Saud Univ. Sci.*, **33**, 101334 (2021); https://doi.org/10.1016/j.jksus.2020.101334
61. M. Bitew, T. Desalegn, T.B. Demissie, A. Belayneh, M. Endale and R. Eswaramoorthy, *PLoS One*, **16**, e0260853 (2021); https://doi.org/10.1371/journal.pone.0260853
62. N. Mani, S. Suresh, M. Govindammal, S. Kannan, E.I. Paulraj, D. Nicksonsebastin and M. Prasath, *Chem. Phys. Impact*, **7**, 100254 (2023); https://doi.org/10.1016/j.chphi.2023.100254